Tellus SERIES A DYNAMIC METEOROLOGY AND OCEANOGRAPHY
PUBLISHED BY THE INTERNATIONAL METEOROLOGICAL INSTITUTE IN STOCKHOLM

# Cyclones, windstorms and the IMILAST project

*By* TIM D. HEWSON[1]* and URS NEU[2], [1]*ECMWF, Reading, UK*; [2]*ProClim-, Swiss Academy of Sciences, Bern, Switzerland*

(Manuscript received 30 December 2014; in final form 28 June 2015)

ABSTRACT

By way of introduction to the TELLUS thematic cluster on outcomes of the IMILAST project (Intercomparison of MId-LAtitude STorm diagnostics), this paper presents the results of new research that is fundamental for the correct interpretation of IMILAST results. Specifically we investigated the mesoscale structure of cyclonic windstorms, and the representation of those windstorms in re-analysis data. The paper concludes with an overview of the project itself. Twenty-nine historic windstorms are studied in detail, using wide-ranging observational data, and on this basis a conceptual model of the life cycle of a typical windstorm-generating cyclone is developed. The model delineates three wind phenomena, the warm jet, the sting jet and the cold jet, and maps out the typical damage footprint left by each. Focussing on the boundary layer, the physical processes at work in each jet zone are investigated. These include the impact of near-surface stability and exposure on gust strength. Based on numerous cases, a generic description of the sting jet is provided, with many new features highlighted. This phenomenon looks to be unique in that exceptional gusts can be realised well inland because destabilisation is activated from above. We next investigate how well the widely-referenced ERA-Interim re-analysis, that has been a primary data source for IMILAST, can represent windstorms. In many ways, performance is suboptimal. Compared to a benchmark manually-analysed dataset, windstorm-generating cyclones generally do not deepen rapidly enough. In part, this is a resolution limitation. For one medium-sized cyclone, it is shown, using other models, that horizontal resolution of order 20 km or better is required to capture the most damaging winds. In the context of IMILAST, which has used data at resolutions $\geq$80 km, this is a fundamental result. For this and other reasons, caution is clearly needed when inferring storm behaviour and severity from model-based metrics.

*Keywords: cyclone life-cycle, conceptual model, sting jet, cyclone tracking, windstorm footprint, satellite imagery, re-analyses, boundary layer, convective instability, evaporation*

## 1. Introduction

Interest in cyclones stems from their innate association with adverse and sometimes disruptive weather. This weather includes windstorms, rainstorms and snowstorms. For the IMILAST project ('Intercomparison of MId-LAtitude STorm diagnostics', first described in Neu et al., 2013), which basically aims to compare different automated cyclone identification and tracking algorithms, the primary driver has been windstorms. This is because of the large societal and insurance losses that can be associated, and because of a related desire to anticipate future changes in frequency. As an introduction to the TELLUS thematic cluster on outcomes of the IMILAST project, this paper provides comprehensive background information on cyclonic windstorms and their representation in models and summarises IMILAST activity to date.

A literature search illustrates that whilst many authors have focussed on structures and physical processes at work in particular evolutionary phases of particular windstorm-generating cyclones, few if any have compared and contrasted the full evolution of a large set of storms. Nor have they generalised their analyses to give a complete picture of the typical life cycle of a windstorm-generating cyclone, from genesis through to decay. So in the first part of this paper, whilst recognising that huge diversity exists, both in extra-tropical cyclone characteristics and definitions, a primary aim has been to construct a useful and general conceptual framework to describe the relationship between cyclone evolution and different classes of windstorms that result at the surface. To do this necessitated comprehensive new investigations of the life cycles of over 20 extreme cyclones.

*Corresponding author.
email: tim.hewson@ecmwf.int



Citation: Tellus A 2015, **67**, 27128, http://dx.doi.org/10.3402/tellusa.v67.27128

To identify and track cyclones automatically, one of course needs input data, and for IMILAST it has mainly been the ERA-Interim re-analysis (ERA-I) (Dee et al., 2011) that has fulfilled this role. Project participants had decided from the outset to use ERA-I as their re-analysis of choice, because of a worldwide reputation for quality. Although re-analysis procedures try to assimilate and dissect as many atmospheric measurements as possible in an optimal way, to create comprehensive gridded datasets, they still have limitations, which relate for example to horizontal resolution (about 80 km in the case of ERA-I). And so with our new conceptual framework to guide, in the second part of this paper we go on to analyse how well ERA-I actually represents cyclonic windstorms. It is of course vital that any users of the re-analysis and the related cyclone tracks fully understand any limitations. We refer also to other higher resolution operational models, to see if they perform better.

To complete the paper, we provide a summary of the results of IMILAST to date, of how the weaknesses identified in lower resolution representations (such as ERA-I) can impinge upon these, and of possible future directions for the project.

A new dataset referred to extensively throughout this paper is the IMILAST storm dataset, or 'ISD', which consists of 22 cyclonic storms that lead to substantial wind-related damage across Europe (see Table 1). These cases shaped our new conceptual model framework and were used as test cases for studying ERA-I fields. The storm list had been pre-selected by IMILAST participants, to try to span as wide a range of storm types as possible. Cases include very small and very large cyclones, impact upon many different geographical areas, and incorporate also two tropical cyclones that underwent extra-tropical transition (ET). Table 1 shows that almost all ISD storms have been referenced before in some form. There were however substantial differences in the extent to which each such study looked at issues relevant to the current paper, with many only touching on these. Regarding the storm names used on Table 1 and throughout this paper, these are based on the assignations of the Institute of Meteorology at Berlin's Free University (though we acknowledge that other institutes across Europe have adopted other names for some storms).

For this paper we enlisted an independent manual re-analysis of the ISD storms, to generate a definitive track and mean sea level pressure dataset with a 6-hour interval – 'best-track' (BESTTRK). The main aim was to define the 'true cyclone behaviour', or as close as one can get to this. As a starting point, we were able to utilise the standard surface analyses manually prepared operationally by senior forecasters, on which isobars, fronts and cyclonic centres are commonly marked. One might argue that a consensus approach which involved scrutinising charts from many European countries would have been best, given that the positions of fronts and cyclones drawn by different analysts can be inconsistent (e.g. see Mass, 1991). However, we instead used UK Met Office charts, because the geographical location of the UK, on the edge of the North Atlantic, and alongside the typical Atlantic storm track, arguably makes accurate representation of Atlantic cyclones and fronts a higher priority there than in many other European countries. Furthermore, the strong cyclones that we are interested in here tend in any case to be associated with strong fronts, which should be more easily and more consistently identified than weaker features. So cyclones on archived Met Office charts, originally prepared in real time by the chief forecaster (an example portion of which is shown at the top of Fig. 3), were the basis of BESTTRK. Importantly, in a second step, these initial BESTTRK estimates were cross-referenced with surface observations (including some that may not have been available to the forecaster at the time), and also with details from the published case studies where they were relevant and reliable. In a few instances this lead to slight adjustments being made to create the final, definitive version of BESTTRK. Only after completing all this did we then employ operational charts produced by another European centre, the Deutscher Wetterdienst, as a quality control, which we discuss in Section 4.

As implied above, throughout the paper we use observations above all else as our analysis tool. By observations we mean the full range – from in situ surface station measurements through to those provided by remote sensing (e.g. satellite and radar). A particular focus has been image sequences from geostationary satellites, many of which were retrieved from the online EUMETSAT archive. Models are used too, but only with caution, recognising that they must contain a sufficiently accurate representation of (and resolution of) key processes, backed up by a highly responsive assimilation scheme, in order to provide analyses and forecasts that correctly mirror observational ground truth. A guiding principle here, which might set this study apart from some others, is that we never accept a model analysis as truth unless there is supporting evidence from the observations.

In our conceptual model of a cyclonic windstorm, we have chosen to have three windstorm classes. Whilst this approach follows the lead of previous authors (e.g. Clark et al., 2005), we have also built substantially on that work in several ways. Evidently far more cases are now used, typical behaviour is being highlighted, and there is a focus on the temporal evolution of each windstorm class and the footprints of damage that they each leave at the surface. Also, given the relative paucity of references to boundary layer processes in previous studies, another aim of this paper is to discuss how such processes impact upon gusts at the surface, highlighting also related differences in vulnerability between windward coasts and other regions. Reference is also made

*Table 1.* Some cyclonic windstorms that have affected Europe

| Name of storm | First impact date | Main countries affected | Storm type (over land) | Some related publications |
|---|---|---|---|---|
| **ISD storms** | | | | |
| Daria | 25/01/90 | UK,NL,DK | W C | Heming (1990); McCallum (1990) |
| Vivian | 26/02/90 | IE,UK,DE,BE,CH,AT,NL | W C | McCallum and Norris (1990) |
| 'Venice92' | 09/12/92 | IT | W | – |
| Lili (ET) | 28/10/96 | IE,UK,DE | C | Agusti-Panareda et al. (2005) |
| Yuma | 24/12/97 | IE,UK | (S) C | Young and Grahame (1999) |
| Anatol | 03/12/99 | DE,DK,SE | S C | Ulbrich et al. (2001); Nielsen and Sass (2003) |
| Lothar | 26/12/99 | FR,CH,DE,AT | W (S) | Pearce et al. (2001); Wernli et al. (2002) |
| Martin | 28/12/99 | FR,CH,DE | C | Ulbrich et al. (2001) |
| Oratia | 30/10/00 | UK | W S C | Hewson (2001) |
| Torsten | 11/11/01 | DZ,ES | C | Tripoli et al. (2005) |
| Jeanette | 27/10/02 | UK,NL,BE,DE,PL,CZ | C | Parton et al. (2009) |
| Quimburga | 20/11/04 | CZ,AT,SK | (W) C | Hewson (2009) |
| Dagmar | 17/12/04 | FR | C | Caspar et al. (2007) |
| Erwin | 08/01/05 | UK,DK,SE,EE | W S C | Baker (2009) |
| Gordon (ET) | 20/09/06 | ES,IE,UK | (W) C | Franklin and Brown (2008) |
| Renate | 03/10/06 | FR | S C | *Ibid* |
| Kyrill | 18/10/07 | UK,DE,CH,AT,DE,PL,CZ | W C | Fink et al. (2009) |
| Paula[a] | 25/01/08 | DE,PL,CZ,AT | W C | Joyner (2013) |
| Klaus | 24/01/09 | PT,ES,FR | C | Liberato et al. (2011); Bertotti et al. (2012) |
| Xola | 23/12/09 | PT | S C | Pinto and Silva (2010) |
| Xynthia | 28/02/10 | FR,DE | (S) C | Lumbroso and Vinet (2011) |
| Ulli | 03/01/12 | UK | S C | Fox et al. (2012); Smart and Browning (2014) |
| **Other storms** | | | | |
| 'October87' | 15/10/87 | UK,FR | S C | Burt and Mansfield (1988); Shutts (1990); Browning (2004) |
| Herta | 03/02/90 | FR,BE,DE | (S) C | Young (1990) |
| Petra | 15/07/10 | UK | S | Wales Online (2010) |
| Friedhelm | 08/12/11 | UK | C | Baker et al. (2013); Vaughan et al. (2014) |
| Christian | 28/10/13 | UK,NE,DK,DE,SE | S C | Hewson et al. (2014) |
| Xaver | 05/12/13 | UK,NE,DK,DE | C | Hewson et al. (2014) |
| Ulla | 14/02/14 | UK,FR | W C | *Ibid* |

List of cyclonic windstorms, in the IMILAST dataset (ISD, top section) and others discussed in this paper (lower section). ET denotes extra-tropical transition case. The likely cause(s) of the strongest gusts *over land*, according to the framework of Fig. 1, are given in the fourth column: W for the warm jet, C for the cold jet and S for the sting jet. Methods of assignation are discussed in the text. Confidence therein is limited by available data, and is subjectively assessed – parentheses indicate 'probable' (50–90% confidence), whilst no parentheses signify 'very probable' ( >90% confidence). [a]Note that damage historically attributed to Paula relates in fact to two cyclones, the one named by the Free University of Berlin that ran east into Scandinavia, and a wave depression that developed later, on its southern flank, over southern Scandinavia, that was not named.

to isobaric patterns, gradients and curvature, in recognition of the key role they play in classical windstorm analysis using synoptic data (see for example Lamb, 1991). Thus, our overall approach in this paper is very pragmatic, trying to bring to the fore surface impacts, explaining them in terms of the driving physics, and describing how they might vary in different scenarios.

Out of the three windstorm classes the most destructive is the 'sting jet' (after Browning, 2004). In recognition, a comprehensive discussion of this phenomenon is included. This highlights a number of important new sting jet properties that have been discovered, and reveals the substantial body of supporting evidence.

The paper is laid out as follows. The new conceptual model is described in Section 2, whilst the evidence on which it was based and the characteristics of the different windstorm zones are in Section 3. Section 4 investigates the ability of ERA-I to represent the ISD storms, and uses other models to discuss one of these in detail, whilst Section 5 focusses on IMILAST activity to date.

The main acronyms used in this paper are as follows (for storm names refer to Table 1):

BESTTRK – Manually-derived TRacKs and central pressures of ISD storms, 6-hour interval

CJ – Cold Jet windstorm phenomenon (Fig. 1)

DCAPE – Downdraught Convective Available Potential Energy
DSCAPE – Downdraught Slantwise Convective Available Potential Energy
ECHAM5 – Version 5 of the European Centre HAMburg model
ECMWF – European Centre for Medium range Weather Forecasts
EUMETSAT – EUropean organization for the exploitation of METeorological SATellites
ERA-I – 'Interim' version of the ECMWF Re-Analysis project
ERATRK – TRacKs and central pressures of the ISD storms, as represented in ERA-I
ET – Extra-Tropical transition of tropical cyclones
HRES – High RESolution (16 km) ECMWF model version
IMILAST – Intercomparison of MId-LAtitude STorm diagnostics (project)
ISD – IMILAST Storms Dataset (22 pre-selected cyclonic windstorms)
SJ – Sting Jet windstorm phenomenon (Fig. 1)
SST – Sea Surface Temperature
UK4 – Met Office UK-centred limited area model (4 km horizontal resolution)
WJ – Warm Jet windstorm phenomenon (Fig. 1)

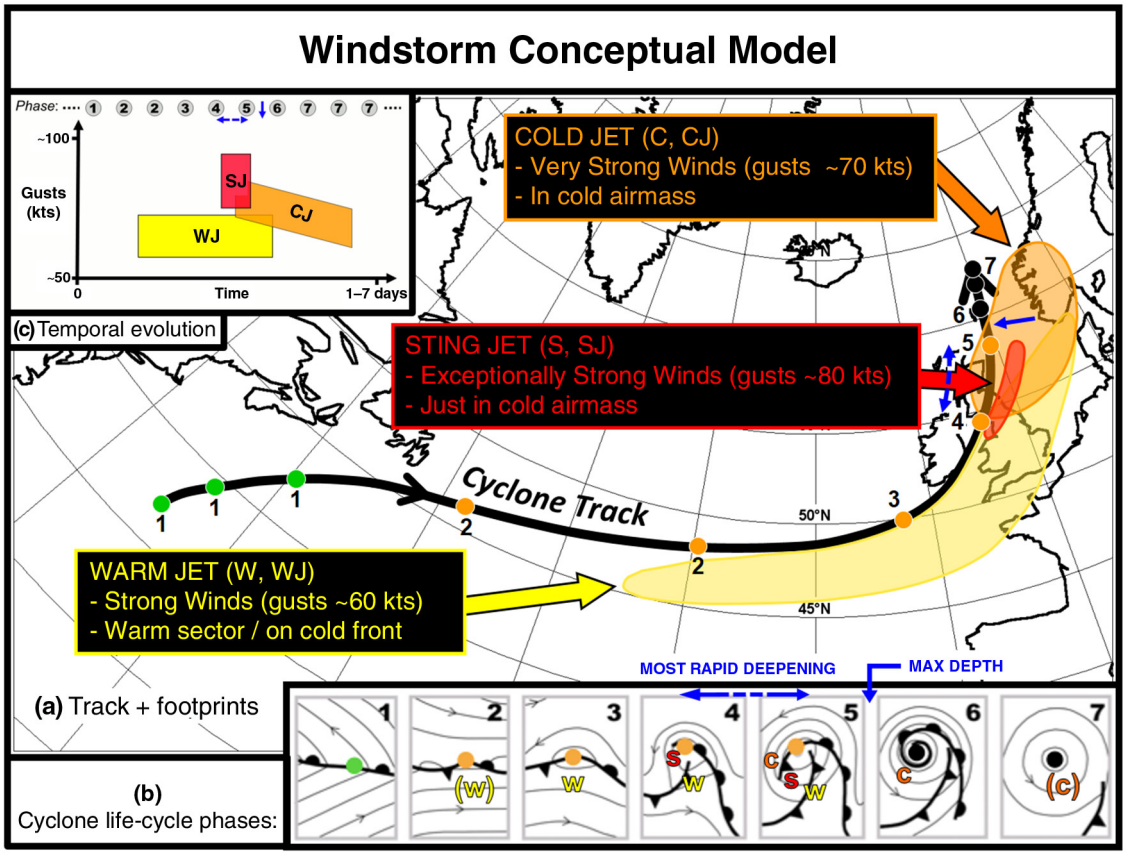


*Fig. 1.* Conceptual model of an extra-tropical cyclonic windstorm. Panel (a) shows the cyclone track (black), with spots denoting positions equally separated in time, and numbered according to the cyclone life-cycle phases in panel (b). Spot colour relates to the identification method and objective typing used in Hewson and Titley (2010), green being a diminutive frontal wave, orange a frontal wave cyclone, and black a barotropic low. Shading denotes the footprints, or nominal damage swathes, attributable to the warm jet/warm conveyor (yellow), the cold jet/cold conveyor (orange) and the sting jet (red). Panel (b) shows the synoptic-scale evolution of fronts and isobars around the cyclone, after Hewson and Titley (2010) and Shapiro and Keyser (1990), with added letters denoting relative locations of the strong wind features, and brackets indicating marginal existence. Panel (c) denotes the temporal evolution of gust strength for each jet zone, with numbers cross-referencing phases on panel (b). On each panel, a dashed blue line denotes the period of most rapid deepening, whilst the solid blue arrow shows the time of maximum depth. This conceptual model should be considered to be *very malleable*; for example most intense cyclones will have only one or two of the three strong wind footprints associated.

## 2. Cyclones and windstorms

The aim in this section is to provide, for damaging extra-tropical cyclones, a unified conceptual model of the structure and temporal evolution of their low-level strong wind zones. Specifically, we have tried to build up an integrated picture of the nominal windstorm footprints, or 'damage swathes', left at the surface as a cyclone translates, develops and decays. This was done because illustrations of net impact in spatial terms, which is of key interest to stakeholders, have historically been lacking. Conversely many previous authors have provided useful snapshots of the low-level strong wind zones, as in Fig. 17 in Clark et al. (2005), and we have adopted their terminology here, referring specifically to three 'windstorm zones': the warm jet (WJ), the cold jet (CJ) and the sting jet (SJ). In putting together our conceptual model we tried to bring together (1) extensive analysis of the ISD and some other cyclonic storms (Table 1), (2) published studies of these cases (last column on Table 1), and (3) new studies of some cases using models with high spatial resolution (e.g. 4 km). Also incorporated were the lead author's 15 yr of experience of dealing with windstorms whilst forecasting at the UK Met Office. So our scientific method has been one of iteration and consilience, accruing evidence from a wide variety of sources, to build up and over time refine our picture of windstorms, in order to arrive at a final conceptual model that is general but also sufficiently flexible to hold fast in the vast majority of past and future cases. The outcomes of this process are presented in the following order: the windstorm conceptual model and descriptions are shown in Fig. 1 and Table 2, which then leads on to detailed discussion in Section 3 where the evidence is documented.

Thus, Fig. 1 depicts the footprints or damage swathes associated with the three windstorm zones (shaded in colour on panel a), connects these to phases in a previously published cyclone life-cycle conceptual model for intense cyclones (panel b, from Shapiro and Keyser, 1990; Hewson and Titley, 2010), and illustrates also temporal evolution (panel c). It is important to appreciate that the extra-tropical cyclone spectrum includes huge variety in terms of structure, size, longevity, and evolutionary behaviour. So the footprints shown in Fig. 1a, which represent an 'average' in most respects, can vary in many ways between cases. Clearly geographical location will change, but the general shapes should also be viewed as being very 'malleable', not only in terms of width and length but also in terms of the degree of curvature of the swathe. For example, whilst most cyclones, during or soon after rapid development, turn poleward and/or decelerate as shown, an important minority do not, and so to encompass those one should envisage the swathe structure *not* curving away to the north, and perhaps being more elongated in the along-track direction at the eastern end. Moreover, whilst all three footprints *can* arise during passage of a cyclone, they will not all be present and noteworthy for every such case; indeed for many windstorms the damage over land is largely attributable to just one of the three classes, as Table 1 examples show. Similarly, in Fig. 1c, the gust levels shown are only indicative of the levels typically attained *inland* for each class when a noteworthy windstorm occurs, and of their relative ferocity. Many cyclones will achieve levels lower than shown, for each category, whilst only a rare few will reach higher levels.

So why do we have three types of windstorm in this conceptual model? The basic division stems from a pattern matching and airmass-based approach, whereby we relate strong winds to their location relative to the positions around the cyclone of fronts, as on Fig. 1b. This approach to windstorm classification also has strong physical significance, because the airmasses that the fronts delineate tend to have very different stability characteristics. In turn, stability defines how easy it is for high momentum air to propagate down, through the lower troposphere, to the earth's surface and thereby elevate gust magnitude. Other defining characteristics then follow on – evidently the relative gust magnitude itself is the one that is paramount, whilst the rarity of, breadth of and duration of the phenomena are others. In addition, trajectory analysis in various modelling studies (e.g. Clark et al., 2005) finds clear distinguishing characteristics for the three windstorm zones. Meanwhile a small point of departure relative to Fig. 17 in Clark et al. (2005) is that the CJ and WJ zones in Fig. 1 extend beyond the immediate vicinity of the fronts, in recognition of the fact that strong gusts and damage can also occur beyond, whilst still residing in the same airmass. Note also that ability to forecast varies with phenomena – the most damaging 'sting jet' phase is undoubtedly the most challenging (see for example the discussion of forecasts for Ulli in Fox et al., 2012). A final, related characteristic, that is key for IMILAST, is how well a re-analysis dataset such as ERA-I can actually represent each zone. This is covered in Section 4.

Due to the iterative way in which the conceptual model in Fig. 1 was constructed, which actually took many years, it is not possible to provide a step-by-step summary of the method of construction. However, we can provide insights into the more systematic way in which the ISD storms were analysed, which clearly fed into Fig. 1, and at the same time also facilitated the new over-land 'Storm type' classifications shown on Table 1. This procedure is outlined on Table 3. Due to both temporal and spatial data discontinuities (such as missing satellite imagery and the fact that observation density varies across Europe) there is inevitably some subjectivity in our classifications, though considerable effort did go into trying to uncover as many data sources as possible, and thereby make the process for each case as complete as possible. As a result, in most instances we were able to

*Table 2.* Key characteristics of windstorms, based around the conceptual model shown in Fig. 1

| | Warm jet (WJ) | Sting jet (SJ) | Cold jet (CJ) |
|---|---|---|---|
| Gust strength | ~50–70 kts | ~70–90 kts | ~60–80 kts |
| Location of strong winds (relative to cyclone and fronts) | Between warm and cold fronts, and on the cold front itself. | Near to the tip of the bent back front, extending NE, E or SE towards the region of frontal fracture. | In cold air encircling the low, initially on the W flank, but moving on with time to the SW, S and SE flanks. |
| Approximate timing of strong winds | Relatively early in the life cycle, but on the cold front somewhat later. Disappears as warm air occludes. | During and just after the period of most rapid cyclone intensification. | Starts out just prior to the time of maximum cyclone depth, then decays slowly. |
| Duration of very strong winds | ~24–48 hours | ~1–12 hours | ~12–36 hours |
| Relative frequency | Fairly unusual | Very rare | Fairly common |
| Stability characteristics | Mostly stable, but pockets of low to mid-level instability possible in warm sector or along cold front. | Cooling through evaporation of cloud head particulate is believed to enhance an instability to downward slantwise convection. | Unstable along onshore coasts; more stable inland, though prone to destabilise here through insolation. |
| Inland versus coastal sites | Stronger gusts on windward coasts where friction lower. Stability effects reduce strength at all sites, though embedded convection can complicate. | Unrelated, due to top-down destabilisation mechanism. So very probably the main driver of extreme gusts inland. | Much stronger gusts on coasts, due to marine (SST-derived) instability. However, insolation may create similar conditions inland by day. |
| Typical relative wind strengths (but can vary) | $V_{GUST} << V_{1KM}$, $V_{1KM} \sim V_G$ | $V_{GUST} \sim V_{1KM}$, $V_{1KM} \sim V_G$ | $V_{GUST} < V_{1KM}$, $V_{1KM} < V_G$ |
| Accompanying weather | Mostly cloudy, rain and drizzle possible, heavier in any embedded convection and on cold front. | Largely dry, broken cloud expected. | Showers likely near windward coasts, possible inland. Cloud usually broken. But thick cloud and heavy rain possible in early stages (cloud head). |
| Footprint width | ~200–500 km (less significant inland) | ~20–200 km | ~100–800 km (may be less significant inland) |
| Footprint length (over land) | Up to ~1000 km | Up to ~800 km | Up to ~2500 km |
| Ease of prediction | Usually straightforward (though cold front gusts more problematic). | Very difficult. | Relatively straightforward, though stability impact can be difficult to gauge. |
| Gusts represented in ERA-Interim? | Yes, generally | No | OK but some weaknesses, especially early on and for smaller systems. |

Summary of key characteristics of the three windstorm phenomena shown on Fig. 1, as deduced primarily from the cases in Table 1. $V_{GUST}$ is wind gust strength, $V_{1KM}$ is the wind speed 1 km above the earth's surface and $V_G$ is the near-surface geostrophic wind speed. Note that the 'Relative frequency' row in the table is intended to be a rough guideline spanning all European cyclones; this differs from the impression given by Table 1 because that shows only pre-selected extreme cases. Characteristics are further discussed in the text.

classify the cause(s) with a confidence level greater than 90%, though for a few confidence is lower (i.e. 50–90%, as signified by parentheses). To illustrate this, an example of the sources of uncertainty for one case is given in Section 3.5.

Table 2 summarises the key characteristics of each of the three windstorm zones. In Section 3, typical cyclone evolution will be described and connected with the three wind phenomena. Many ISD examples, listed in Table 1, will also be used as evidence. An important consideration, when referring back to studies of these past cases (column 5 of Table 1), is that the scope and extent of those studies varies. Similarly one cannot of course expect old research to have embraced newer concepts – the SJ, first highlighted by Browning (2004) and that we discuss below, is the main example. So for these differing reasons the extent to which past paper contents supports our assigned 'cause' (column 4 of Table 1) inevitably varies. Furthermore, in the case of cyclones Erwin and Ulli, our inferences are somewhat at odds with those found by other authors and this we discuss in Sections 3.3.4 and 4.2 respectively.

*Table 3.* How the causes of peak gusts over land were assigned

| Checklist of steps for assigning peak gusts to WJ, SJ or CJ for a given cyclone |
|---|
| 1. Refer to BESTTRK data to ascertain cyclone timing. |
| 2. Examine surface observations (from various sources*) over land to ascertain peak gusts associated with the cyclone (referencing step 1) and the times when they occurred. |
| 3. Obtain (from various sources**) synoptic chart sequences at $\leq 6$ h intervals, to span the time of the peak gusts (from step 2), in order to document where, relative to front and cyclone positions, the peak gusts occurred. |
| 4. Assign each of the peak gusts to one of the following three categories:<br>**WJ**: If the gust was in the warm sector or on the cold front (stages 2,3,4,5 on Fig. 1b).<br>**CJ**: If the gust was in the cold air behind the cold front and either (1) this gust was situated more than 300 km from the tip of a bent back front/occlusion or frontal wave, and/or (2) the bent back front/occlusion extended more than 300° around the low centre, as measured from the bearing of the triple point. (5, 6, 7 on Fig. 1b).<br>**CJ** *or* **SJ**: If the gust was in the cold air behind the cold front, and neither (1) nor (2) immediately above were satisfied. |
| 5. For cases in the 'CJ *or* SJ' category investigate in detail whether a SJ was the likely cause, using wide-ranging data, as available, and following the detailed guidelines regarding SJ hallmarks presented in Section 3.3. Accordingly where SJ probability is subjectively deemed to be greater than 50% assign SJ as the cause, otherwise assign CJ. |

Shows the process by which the causes of peak gusts over land (WJ, SJ, CJ) for the windstorm-generating cyclones examined for this paper (Table 1) were ascertained. At step 2 the data sources (*) included standard observations circulated in real time via the global telecommunications system (GTS), observations documented in references on Table 1, autographic records obtained separately (e.g. Fig. 9b), and observational evidence documented on web sites (e.g. www.meteo-paris.com/chronique/annee/yyyy, where yyyy is the year). At step 3 sources (**) included Met Office surface analyses (recent years online at www2.wetter3.de/Archiv/archiv_ukmet.html), surface analyses from references in Table 1, analyses drawn manually for this paper, and objective synoptic charts from the ECMWF model (based on Hewson, 1998).

To generate a noteworthy windstorm, simple geostrophic arguments and experience lead one to conclude that ordinarily a cyclone has to undergo a period of rapid development, with a major reduction in central pressure and/or a marked increase in lower tropospheric vorticity around the centre. Often we are dealing with 'bombs', that is cyclones that deepen at a rate of more than about 24 hPa in 24 hours (at 50°N) – see Sanders and Gyakum (1980) for the full definition. The blue arrows on Fig. 1 relate, showing where and when maximum depth (solid) and maximum deepening (broken) typically occur, though again these will vary between cases. On Fig. 6, to be discussed fully later, note how for most of the ISD cases the end of the period of most rapid 6-hour deepening (shown by pink circles) comes shortly before the time of maximum depth (0 hour on x-axis). In 70% of cases the gap is 12 hours or less, and indeed in 30% it is zero.

## 3. Cyclone evolution, and evidence for windstorm zones

### 3.1. Introduction

Whilst accepting that the definition of exactly what constitutes a cyclone is not clear-cut (as discussed also in Section 5) we take here a synoptic standpoint, and adopt the conceptual model framework shown in Fig. 1b, which permits a cyclone to start out as a diminutive wave (green spot) or a frontal wave (orange) or even, rarely, as a barotropic low (black). In a random sample of cyclones in Hewson (2009) over an extended North Atlantic domain, the proportions that started out in these categories were 53, 30 and 17%, respectively. Within this framework, as opposed to one that relied solely on pressure minima for example, the majority of windstorm-inducing cyclones that affect Europe undergo genesis in the western North Atlantic. Some notable examples include the Great October Storm of 1987, Lothar in 2000, and Christian and Xaver in the winter of 2013/14. Some also form closer to Europe however: Quimburga that delivered damage of apocalyptic proportions to high level forests in Slovakia, Renate that hit central France, and Xola that struck Portugal all formed east of 25°W, and these are all in the ISD.

Though it is beyond this paper's scope to discuss in any detailed way the atmospheric dynamics that lead to the rapid intensification of these incipient cyclones, which by definition tend to start out as weaker features, as background it is useful to highlight a few key points regarding the role of the broadscale flow. It is a very commonly held view that there needs to be some upper level driver for development; a pronounced upper level trough and/or a strong upper level jet. As the trough catches up and interacts with the cyclone, and/or the cyclone crosses the jet core, substantial cyclogenesis can ensue. Numerous papers discuss these processes, for example McCallum and Norris (1990) highlight the primary importance for European cyclonic windstorms of *confluent* upper troughs, whilst the idealised primitive equation simulations of Schultz and Zhang (2007) support

this finding – they show how the confluent trough scenario favours development of the damaging Shapiro-Keyser type of cyclone (as used in Fig. 1). Meanwhile Baehr et al. (1999), Wernli et al. (2002) and others focus on jet crossing. Latent heat release is a key component too, perhaps contributing between one half and one third of the full deepening of a cyclone (as in Shutts, 1990; Nielsen and Sass, 2003). Other dynamic and thermo-dynamic factors that may play a key role in the cyclone's SJ phase are referred to in Section 3.3 below.

Subsections that follow refer extensively to Figs. 2–4. These show sample soundings for each of the windstorm phenomena, a synoptic chart and weather station observations during passage of a windstorm, and 'damage footprints' left at the surface by three storms, respectively. On Fig. 4, letters have been added to indicate the likely cause of the strongest gusts (see Table 3).

### 3.2. *Warm conveyor belt jet (WJ)*

Many windstorm-inducing cyclones move slowly initially, perhaps in the right entrance of a strong cross-Atlantic upper level jet, before accelerating into the jet core. In the ISD, 62% exhibit such acceleration. The spot markers on Fig. 1a signify cyclone positions equidistant in time, so the spacing increase near Newfoundland is indicative of this behaviour.

It is during rapid cyclone translation, in phases 2 and 3 on Fig. 1, that the first windstorm footprint sometimes develops, in the warm conveyor belt region (or 'warm jet' zone = WJ). With thermal gradients being very small, here the thermal wind relationship implies little vertical shear in the warm sector, and if the upper jet is very strong, then wind speed above the friction layer, say at 1 km ($=V_{1KM}$), can be very strong too $-70$ knots is not that uncommon. Winds on the WJ sounding in Fig. 2a exhibit these various characteristics: no directional shear and speed variations largely confined to lower levels.

As isobars are often straight in warm sectors, $V_{1KM}$ can also appear surprisingly strong relative to the isobaric spacing, or geostrophic wind speed $V_G$. This is because for straight flow typically $V_{1KM} \sim V_G$, whilst in other parts of a cyclone, where isobars are mostly cyclonically curved, one commonly sees $V_{1KM} << V_G$. Conversely, in winter at least, warm sectors in the broader European area are usually stable at low levels, due to cooling from the land or ocean below, a factor that strongly inhibits the downward transfer of momentum to the surface. This stability is clearly visible on Fig. 2a, represented by the increase in potential temperature with height. Similarly, friction decelerates the wind more in stable than in unstable situations, so inland from exposed coasts WJ gust activity is typically even less marked. Examples of cyclones generating WJ gusts in southern England include Ulla on 14 February 2014 (top of Fig. 3), and Oratia in October 2000 (as reported in Hewson, 2001, and as represented on Figs. 2a and 4b).

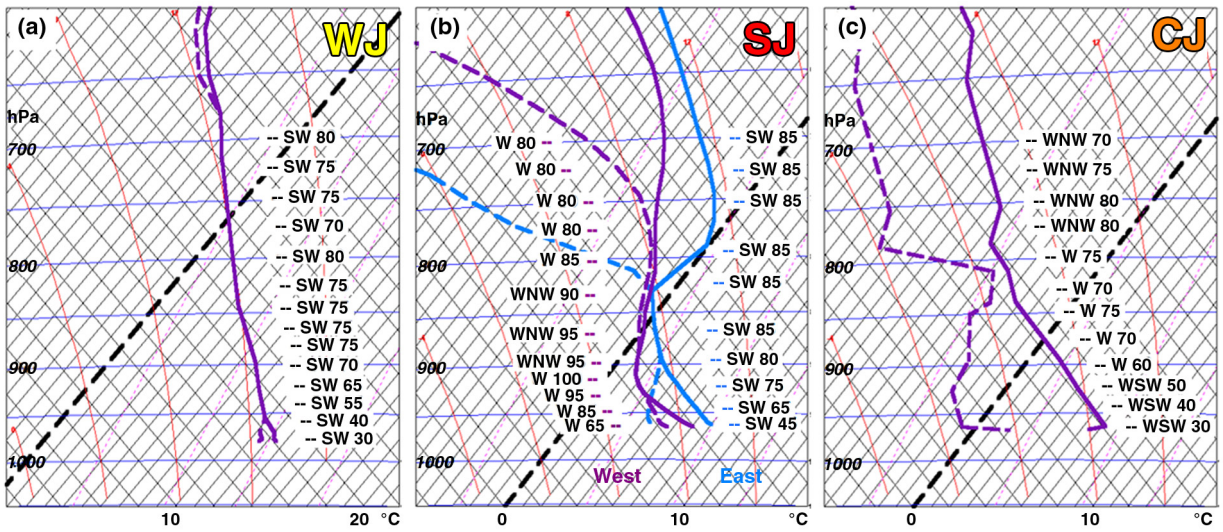


*Fig. 2.* Example UK-area lower tropospheric soundings for the WJ, SJ and CJ phenomena, in (a), (b) and (c), respectively, with winds in alphanumeric format (speeds in kts). Pressure in hPa is shown on the left, whilst temperature in °C is shown below. (a) is for Camborne at 00 UTC on 30 October 2000 (Oratia), whilst (c) is for Crawley at 18 UTC on 25 January 1990 (Daria). To denote the SJ (b) shows two soundings from ECMWF HRES 6-hour forecast fields valid at 06 UTC on 3 January 2012 (Ulli). These nominally straddle the SJ surface impact zone at this time; mauve is to the west, blue to the east. Sounding locations are shown (by coloured rings) on Fig. 4b for the WJ in (a), on Fig. 10b for the SJ in (b), and on Fig. 4a for the CJ in (c).

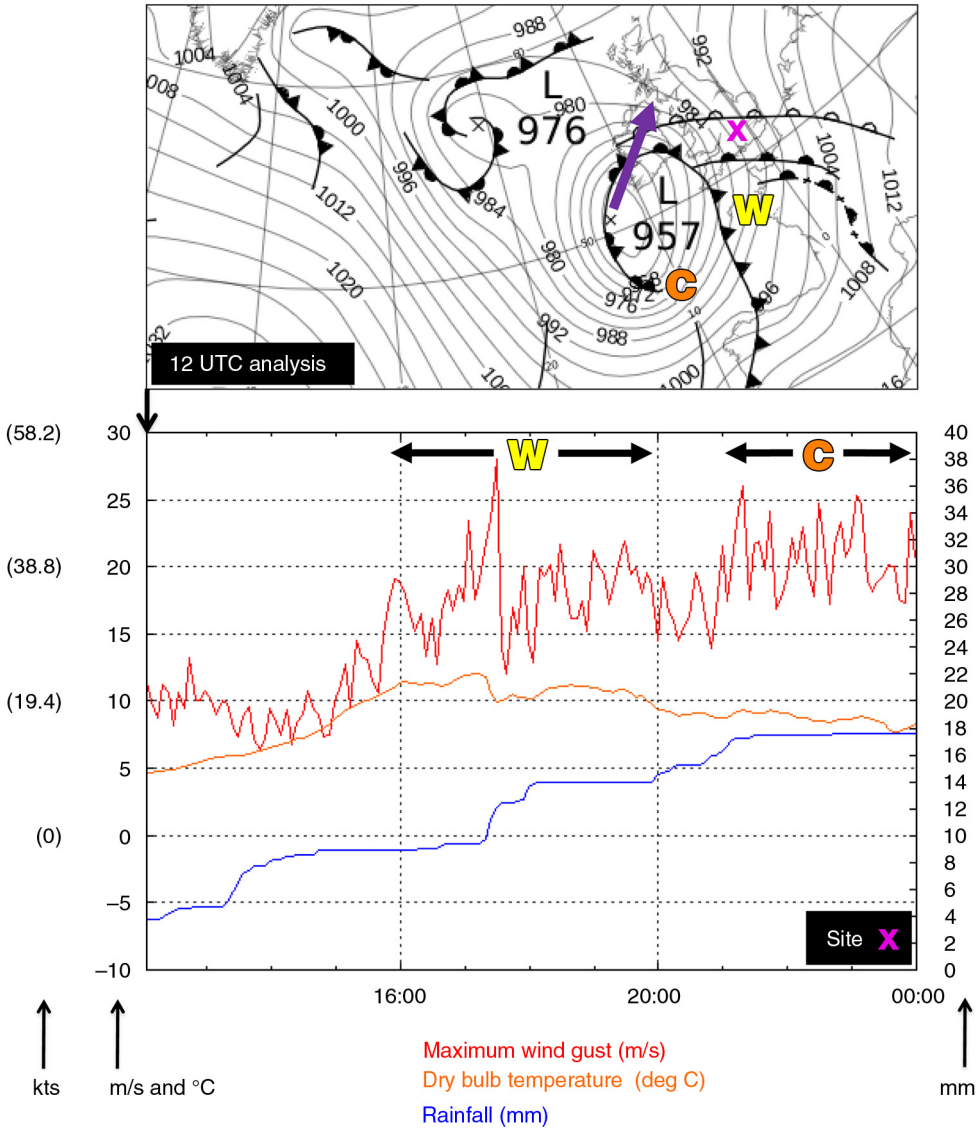


*Fig. 3.* Top panel shows a portion of the Met Office synoptic analysis chart for 12 UTC on 14 February 2014; Ulla (Table 1) is the cyclone southwest of Ireland. A purple arrow shows the 12-hour movement of Ulla whilst 'W' and 'C' denote the centres of, respectively, the WJ and CJ phenomena at 12 UTC. A pink cross marks the Reading University Atmospheric Observatory. Panel below shows observations from this Reading site for the same date, as Ulla advanced northeastwards. Red shows gust strength (m/s and kts, left axis), blue shows accumulating rainfall total for the day (mm, right axis) and orange shows screen temperature (°C, left axis). Time on the x-axis is UTC. Labelling at the top denotes the approximate durations of the warm and cold jet phenomena at this site, as inferred from the traces and synoptic pattern. (The lower panel is reproduced with permission from Reading University Department of Meteorology).

For both Oratia and Ulla, gusts reduced from about 70 kts on the coast to approximately 40–50 kts about 100 km inland. Indeed the low-level reduction in wind strength on Fig. 2a is probably less than it would have been had the site been further inland (for southwesterly flow the coast is only about 15 km upwind). Note also that in WJ cases cloud cover that is commonplace (again reference Fig. 2a) tends to inhibit any destabilisation via insolation. This denotes a positive feedback because the cloud is partly associated with cooling from below, a process which is at the same time stabilising the lower troposphere.

Although marked inland reduction of WJ gusts is common, it is however possible for such gusts to be elevated by downdraught activity related to convection. Such downdraughts

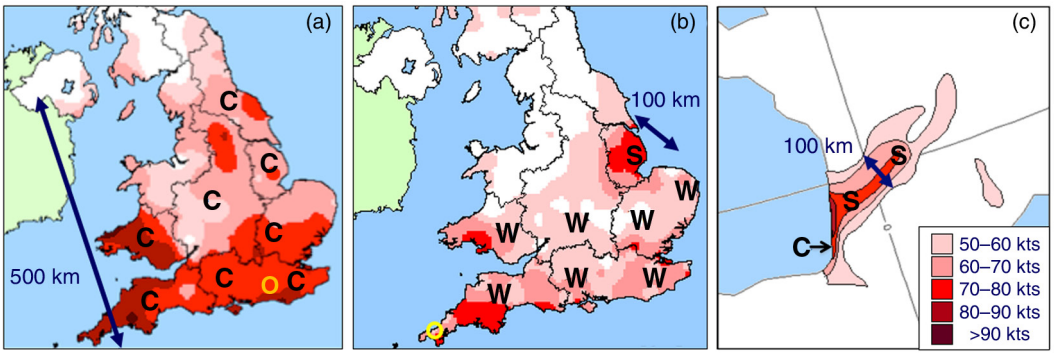


*Fig. 4.* Maximum wind gusts (kts) observed during the passage of three ISD cyclones (Table 1); Daria in (a), Oratia in (b) and Renate in (c). Letters denote the assigned cause of the maximum gust in different regions (W for warm jet, S for sting jet and C for cold jet). Orange and yellow rings on (a) and (b) respectively denote the locations of Camborne and Crawley; soundings from these sites for the said windstorms are shown on Fig. 2c and 2a, respectively. (Panels a and b are reproduced with permission from the Met Office).

bring with them momentum associated with the broader-scale synoptic pattern. This complication may arise when mid-level instability is being released within the warm sector (there are hints of such instability in the saturated air on Fig. 2a, between 900 and 700 hPa), or when there is active convection, perhaps line convection, on the cold front (at the western end of the warm sector), which we have classed as a WJ phenomenon as the warm air is the likely source of the strong winds. To illustrate surface impact, the lower part of Fig. 3 shows observations from Reading on 14 February 2014, on the southeast flank of cyclone Ulla. The temperature trace suggests that the warm sector lasted from about 1600 to 2000 UTC. Cumulonimbus clouds overhead at around 1725 UTC generated very heavy rain and also caused a *transient* but very marked increase in gust strength. From the rainfall trace (and radar data not shown) the apparent time of cold front passage (around 2000 UTC) was relatively inert however, explaining the much weaker gusts at this time. Meanwhile Pearce et al. (2001) provide evidence of extreme 93 kt WJ gusts during cold front passage through Orly airport near Paris, as Lothar's centre passed by just to the north. The thunderstorm also observed strongly suggests a convective contribution. Similarly, for Vivian, McCallum and Norris (1990) report the cold front to be a primary location of very strong gusts, whilst Fink et al. (2009) highlight a similar association for Kyrill over mainland Europe.

As the parent cyclone deepens and transfers east, there may be a tendency for warm sector pressure gradients and therefore WJ gusts to increase. However, this can be counteracted by the narrowing (west to east) of the warm sector, and by migration of this sector away from the parent low, as illustrated by phases 4–7 on Fig. 1b, and by the tapering of the footprint near Denmark on Fig. 1a. Hence the warm sector gust level is constant on Fig. 1c. Warm sector narrowing happens in tandem with what is often termed the 'occlusion process', and indeed whilst Fig. 1b shows no occlusion as such, note that Schultz and Vaughan (2011) propose an equivalent figure in which an occlusion replaces the bent back front from the location where warm and cold fronts almost meet, so this is a moot point.

### 3.3. *Sting jet (SJ)*

*3.3.1. Introductory remarks.* Over the last 10–15 yr, evidence has built up in the literature, and in observations, that a small subset of extreme cyclones can have a short period of exceptionally strong winds associated. Following Browning (2004), we are referring here to the 'sting jet' (SJ) phenomenon. Figure 1 indicates that for a given cyclone the SJ, if there is one, will occur briefly, generally during and just after the period of maximum deepening, and just before the cyclone reaches its maximum depth, essentially between cyclone phases 4 and 5. As the SJ is such a destructive feature, as few if any previous studies have examined so many cases using so many different observational data sources, and as there are many new results, this subsection (3.3) necessarily includes extensive discussion.

Whilst research elsewhere continues to identify specific SJ cases (e.g. Parton et al., 2010), the three-dimensional trajectories of air parcels that are involved (e.g. Clark et al., 2005; Martinez-Alvarado et al., 2010), the processes on which SJ existence probably depends (evaporation, slantwise convection, etc., e.g. Gray et al., 2011), and the climatological distribution and frequency (e.g. Martinez-Alvarado et al., 2012), here the focus is very much on the surface impact. Recognising also the difficulties that models have in representing SJs and gusts in general, partly because of resolution (see Martinez-Alvarado et al., 2012, and Section 4 below) and partly because of boundary layer parameterisation issues (e.g. see Parton et al., 2009; Smart and Browning, 2014) we again bring observational evidence

to the fore, specifically surface station data and satellite imagery. So for our purposes a SJ zone will be broadly defined to be:

> a small region affected by exceptionally high surface wind gusts, that occurred close to but downstream of the tip region of a cloud head of a cyclone that was undergoing, or had very recently undergone, rapid intensification.

This definition is consistent with the SJ picture portrayed in other publications, including those mentioned above, and indeed with the picture that emerges through the iterative process of studying many cases (Table 1). In classifying some of these cases as possessing a SJ over land, we had looked in addition for other hallmarks, such as evaporating tips from the cloud head, and notably a propensity for gust strength to be unaffected by passage inland. These aspects are all discussed below.

Attempts to find real sounding data within a zone where a sting jet was clearly impacting the surface failed, due to SJ rarity, sounding sparseness, and sonde release difficulties during extreme winds. So instead to illustrate we show in Fig. 2b two model soundings from the Ulli SJ case. These lie just to the west (purple) and just to the east (blue) of the region where the most extreme winds would affect the surface. They are discussed further below, in Section 3.3.5.

Finally here note that whilst the vast majority of SJ cases, and cyclonic windstorms for that matter, occur in the winter half of the year, we have deliberately also included on Table 1 a case that occurred in summer (Petra), to highlight that SJs are not purely a winter-time phenomenon. Other extreme windstorms to have occurred in summer include the famous 'Fastnet Storm' of August 1979 (Pedgley, 1997), though satellite data coverage issues precluded revisiting that particular case in a consistent way here.

*3.3.2. Surface observations.* As implied above spatial maps of maximum gusts and satellite imagery sequences can both show striking signatures of a SJ. Figure 4 shows the maximum gusts observed for two storm cases which we believe had SJs associated: Oratia in (b) and Renate in (c), whilst Fig. 9a, to be discussed in detail in Section 4, shows surface SJ observations for Ulli (enclosed by the red line). The SJ footprints for these and other cases exhibit noteworthy characteristics (Fig. 1 and Table 2) as we now discuss.

The first important SJ characteristic is the breadth of its footprint (red zone on Fig. 1a), which can vary but which is usually relatively small. Examples include 200 km for 'October87', 150 km for 'Herta', 90 km for Oratia, 40 km for Renate and Ulli, and about 25 km for Xola. To a first approximation breadth reflects cyclone size. At peak intensity, for example, the approximate diameters of the largest closed isobar for the six cyclones above were 600, 600, 600, 150, 400 and 300 km, respectively. The fact that even very small systems can give rise to substantial SJ gusts is also striking. Even more striking perhaps is the fact that the most extreme of these six cyclones (Xola) appears to have been one of the smallest. Pinto and Silva (2010) report a primary damage swathe for Xola measuring about $50 \times 25$ km, in which 10 m gusts, carefully derived from calibrated Doppler radar data, were a phenomenal 100–125 kts.

From an impact perspective a second, fundamental characteristic of the SJ footprint is that its intensity does *not* reduce to any great extent moving inland (until, of course, the feature ceases to exist). Note how gusts of 70–80 kts or more are maintained well inland on Figs. 4c and 9a, and actually develop inland (as the SJ develops) on Fig. 4b. This sets the SJ apart from the WJ and CJ phenomena. Further evidence of this difference can be seen in observations for windstorms Christian and Xaver, as discussed in Hewson et al. (2014); Christian, a SJ case, exhibits almost zero along-flow reduction over land, whilst for Xaver, a CJ case, there is a marked reduction. The reason is probably that the momentum giving rise to the SJ gusts is to an extent propagating downwards in airstream form, in a dynamically forced sense (perhaps in the manner proposed by Schultz and Sienkiewicz, 2013). Mechanisms are discussed in Section 3.3.5.

The third characteristic to note (as shown on Fig. 1c in particular) is that the SJ zone can develop *suddenly*, in both a Lagrangian and an Eulerian sense. Respectively, this means that strong winds do not necessarily move in from somewhere else, and that the period in which the gusts increase at a site can be very short indeed. Storm Oratia provides evidence of sudden development in the Lagrangian frame – note the sharp back edge (western side) to the SJ region over eastern England on Fig. 4b. The low centre was $\sim$200 km to the north and moving northeastwards at the time, as on Fig. 1a. Further supporting evidence of the sudden onset of SJ gusts for Oratia (in a three-dimensional Lagrangian sense) is the complete absence of winds of gust-level strength anywhere in the low and middle troposphere, just 1–2 hours before, upstream at the Aberystwyth Mesosphere Stratosphere Troposphere (MST) radar site in west Wales. Figures in Browning (2005) and Parton et al. (2010) suggest a tropospheric wind maximum then of just 50–60 kts, thereby implying a remarkable intensification rate for this maximum of order 30 kts/h. Nielsen and Sass (2003), in studying Anatol, also remark on the sudden onset of very strong winds near the bent back front. For storm Ulli, to be discussed in detail later, such was the rapidity of the onset of strong winds in the Glasgow area (see Fig. 9b) that a roar could be heard just in advance (Peter Sloss, personal communication). This of course is

rapid onset in the Eulerian frame. In parallel, these various observations also suggest that trajectory analysis of SJ cases might benefit considerably from a short time step, ideally far less than 1 hour.

For forecasters, the sudden onset of a SJ is one aspect that makes accurate prediction critical, but at the same time extremely difficult; the small scales involved, the short duration and the difficulties that many models have in process representation only compound this difficulty.

The final noteworthy SJ-related features of surface observations are temperature and wind direction. The SJ zone is in a frontal fracture region, potentially with cold fronts ahead of and behind (phases 4 and 5 on Fig. 1b), so screen temperatures tend to fall somewhat during SJ passage, and then plateau out, at a lower level, after the SJ has moved on. Similarly, there is ordinarily a first clockwise wind shift on the main cold front, just before SJ arrival and a second clockwise wind shift, on the bent back cold front, after the SJ has passed. Smart and Browning (2014) discuss using these aspects to isolate the SJ for Ulli.

*3.3.3. Isobaric pattern*. The area with the smallest isobaric spacing (i.e. largest $V_G$), which is also usually a region with large (cyclonic) isobaric curvature, tends to lie slightly upstream of the SJ surface gusts (e.g. Fig. 1b, phase 4). In the SJ zone itself, gradients are usually a little less and isobars markedly straighter; these isobars tend to splay out downstream. Such a structure can be seen, for example, in storms Ulli (Fig. 10b, between the blue and purple rings), Oratia, Herta and October87. The presence of only small curvature within the SJ zone may be key; it renders the gradient wind as approximately equal to $V_G$ (similar to the WJ) whereas upstream where gradients are largest gradient wind will generally be less than $V_G$ due to the curvature.

*3.3.4. Imagery signatures*. As highlighted by Browning (2004) and others infra-red imagery sequences can exhibit clear signatures of SJ air parcels descending from within the cloud head. Typically one sees one or more cloud filaments in the cloud head tip region. These sometimes dart forward, in pulses, yet each time also appear to dissipate (i.e. evaporate and/or warm). The visual impression one gets can be like that of a 'smoking gun'. One such filament can be seen for Renate on Fig. 5a (blue outline) – animations showed this to be advancing only slowly at this time, much more slowly in fact than the near-surface winds, implying evaporation. Perhaps more importantly, gaps or furrows are maintained between or adjacent to filaments, and sometimes these extend forwards into holes in the low-level cloud deck (most clearly seen on any available visible imagery). One such gap/hole is highlighted with a closed dashed green contour on Fig. 5a, with the enlargement on Fig. 5b showing clearly that the highest brightness temperatures coincide. Out of the SJ cyclones examined, many had only one or two cloud head tips and gaps, though for larger systems such as October87, Anatol and Erwin there were rather more.

As the smoking gun effect and the appearance of gaps/holes are both believed to be symptomatic of descending SJ trajectories, and evaporation, they should also be hallmarks of elevated surface gusts. Indeed Browning (2004) highlighted a strong connection between the strongest gusts in surface observations, and the close proximity, upwind, of filaments in the cloud head tip region for October87. A careful comparison for Oratia in the SJ zone over eastern England (Fig. 4b) takes this a stage further, showing that the highest gusts actually occurred downwind of the *gap* regions. The beginnings of the SJ phase for Christian, over southern England, were also signified by elevated gusts clearly occurring in gap regions (on high-resolution radar imagery), as reported in Hewson et al. (2014). Also for Renate (Fig. 5a and b) note that the main cloud gap lies exactly at the beginning of the central axis of the SJ footprint (double red line). Meanwhile Ulli and Petra also show similar characteristics, except that the most marked gaps/holes, where some exceptional gusts were registered, was on the equatorward side of the primary cloud head tip (e.g. Fig. 9c for Ulli). Some of the most compelling evidence is provided by the much more spatially continuous Doppler radar presented in Pinto and Silva (2010) for Xola. On several of their plan-view snapshots it is striking how the strongest winds are seen around where the signal disappears due to lack of precipitation — that is, the gaps. The general observation that gust maxima are in/downwind of gaps is fully consistent with the airflow schematic in figure 14 in Browning (2004), specifically the cross-section 'N-L' which shows descent in both filament and gap regions, but more pronounced descent in the latter. What is new here is that a relatively large body of new supporting evidence has now been uncovered.

Comparison of Fig. 5a and 9c also indicates very different lengths (downstream) for the gap and filament regions, about 60 and 200 km for Renate and Ulli, respectively. These and other cases suggest this may simply relate to cyclone size. The length difference could at the same time be symptomatic of different descent angles/rates for the sting jet pulses themselves. Note also that short filaments/gaps on satellite imagery may *look* less convincing to the analyst, though they are probably no less important.

One should also ask where the filaments in the cloud head tip come from. In the cases studied, there seem to have been two types. The first type of filament appears to form in situ within the broader tip region of the cloud head, in tandem with the adjacent appearance of furrow(s)/gap(s).

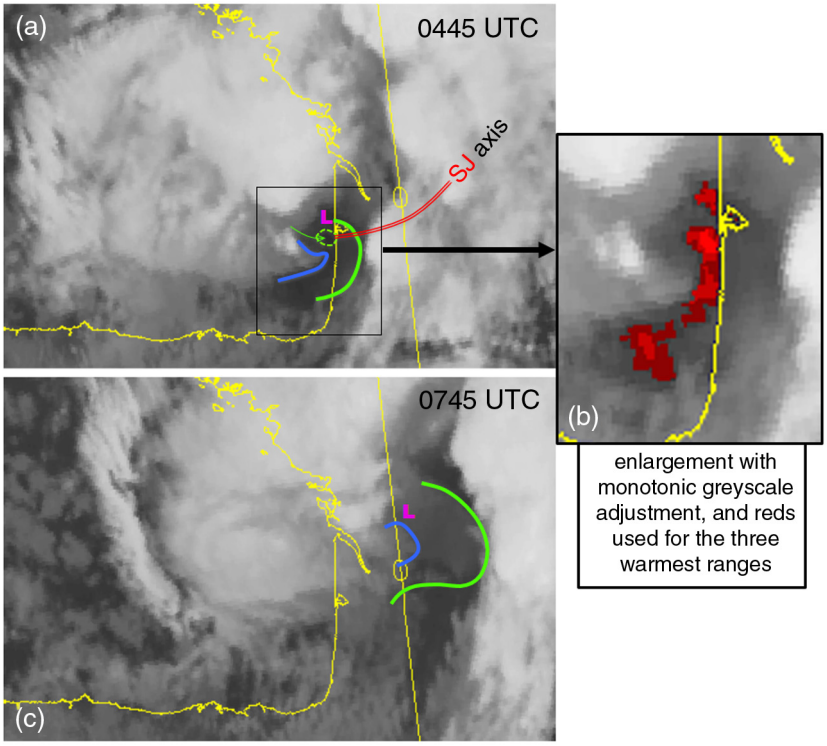


*Fig. 5.* Meteosat infra-red images during the passage of windstorm Renate (Table 1) on 3 October 2006, at 0445 UTC (a), with an enlarged portion in (b), and 0745 UTC (c). L denotes the low centre and the blue line denotes the evolving edge of the cloud head tip. The solid green line denotes the forward edge of an advancing low-level cloud sheet which had breaks in at the earlier time; the closed dashed green contour highlights the most clear-cut break [brightest red on (b)]. The green arrow aligns with a gap/furrow of warmer cloud tops in the cloud head. This furrow is believed to be symptomatic of a descending pulse of high momentum air – the SJ – that is moving in the direction of the arrow, faster than the low centre is moving. The double red line is the axis along which the maximum SJ gusts occurred (from Fig. 4c).

The second type however has clearer origins that are more consistent with the Browning (2004) model, that show up on imagery as the pulsing tail end of a much longer curved narrow band of cold cloud tops and high surface precipitation rates. Each such band would previously form as an arc on the inside edge of the cloud head and then slowly propagate away from the (low) centre, like a ripple formed by a stone dropped into a calm pond. From a process perspective the filaments thus denote the descending remnants of a previously rapidly ascending, tilted, cyclonically curved thin sheet of saturated air, which may have come into existence as a burst of (slantwise) line convection near the bent back front. Such a sequence of events can be seen in radar data over southern England as Christian develops.

In discussing storm Erwin, Baker (2009) suggests that the SJ for that case was weaker than the CJ, based mainly on model simulation figures shown for 850 hPa at a particular time. However, if imagery is compared with surface observations over time during the passage of Erwin, two pulses of very strong gusts can be detected. The first occurred on a cold front (i.e. WJ), around the time of the Baker plot, whilst the second, that was stronger, came about 3 hours later, just ahead of the cloud head tip region (i.e. SJ), as filaments and gaps became more prominent in that tip region. Two notable temperature drops occurred. The first, unsurprisingly, was on the cold front. The second came after the second pulse of gusts had passed, consistent with assignation of those gusts to the SJ. It may be that this SJ maximum did not appear on the published model plot because of sudden onset similar to that discussed in 3.3.2 for Oratia, and/or because of simulation imperfections, and/or because winds ended up stronger below 850 hPa as the SJ descended and accelerated. In the Doppler radar SJ scan for Xola in Pinto and Silva (2010), winds were about 15 kts *less* at 1500 m altitude than at 550 m (the lowest level). And as discussed in Section 2 differing stability characteristics mean anyway that the way that 850 hPa wind speeds might map onto surface gusts can vary greatly according to one's location relative to cyclone and fronts (an aspect also remarked on in Clark et al., 2005). Baker highlights that more work is needed in this area, a point that we support.

For SJ cases, a final noteworthy aspect of imagery sequences is the fact that the 'smoking gun' (SJ) phase, where the cloud head tip region remains in a relatively steady system-relative position, is quite short. Commonly it lasts only a few hours (as for Oratia and Renate), or in extremis may continue for say 12 hours (October87). Termination denotes the end of SJ-related gusts at the surface. So the ultimate length of the SJ footprint will be the mathematical product of the SJ duration (or 'smoking gun' phase on imagery) and the translation speed of the responsible cyclone. Figure 1a depicts a typical length (and breadth).

As the SJ phase terminates, image sequences show cloud from the cloud head tip region to *advance* around the low, as any evaporation and pulsing come to an end. Any holes in the low-level cloud fill in, and this newly homogeneous low-level cloud, together with the colder tops from the cloud head, tend to advance together and will sometimes also expand laterally to form a hammerhead shape on the eastern flanks of the cyclone centre. This evolution is illustrated by comparing Fig. 5a and c for Renate; note how the low-level cloud (west of the green line) advances forwards of the low with holes filling in, whilst the cloud head tip (blue line) loses its definition somewhat and starts to blend in. Petra and Ulli provide further examples, with clear-cut hammerhead cloud patterns developing (not shown). It is also worth remarking that Erwin showed a more complex evolution that provides a cautionary note for forecasters; there were early suggestions of cyclonic wrap-up, but then the cloud head tip region re-asserted itself. This behaviour may relate to the presence of a double frontal structure (which should be considered a rare variant on the picture shown on Fig. 1) though how pivotal that aspect was is far from clear.

Note also that notional SJ footprints probably occur much more often over the ocean than over land (as suggested also by Martinez-Alvarado et al., 2012) – Klaus for example appears to have had a SJ over the ocean but this decayed before reaching land (recall that on Table 1 we classify by gusts observed over land).

*3.3.5. Stability and the downward propagation of momentum.* Schultz and Sienkiewicz (2013) hypothesize that in the SJ zone continued momentum propagation to the surface, and hence high surface gusts, are aided by convective overturning, which in turn is fuelled by instability caused by the relatively high temperature of the underlying surface [Sea Surface Temperature (SST) in their case]. This may be of relevance over the ocean, as for the CJ (Section 3.4.2). However, it cannot be a factor for cases over land when solar heating is nil or negligible (as was true for 77% of the SJ cases on Table 1, including Renate, Oratia and Ulli), so it seems that one or more different processes must be at work here instead, to assist with the downward propagation.

It has been proposed (e.g. Gray et al., 2011) that descent from within the cloud head is aided by the along-trajectory release of downdraught slantwise convective available potential energy (DSCAPE). This implicitly includes the cooling of air parcels by evaporation of cloud head particulate (water or ice) contained therein, and may also be boosted by evaporation of additional particulate added from above. In these ways, it would seem, the usual impediments to the downward transfer of momentum, notably stability and friction, can be overcome, from above, in a systemic way. Model evidence across studies remains somewhat inconsistent however. For example, Martinez-Alvarado et al. (2010) found different vertical structures of jets in simulations of one case by two different models, whilst Smart and Browning (2014) found little evidence of an evaporative contribution in their simulations of Ulli. Indeed all previously published simulations, to the authors' knowledge, failed to resolve/show the ubiquitous SJ hallmarks one sees on imagery. By this we mean the fine-scale filaments and gaps in the cloud head tip area, evaporation of particulate in both such regions, and gust maximisation downwind of the gaps.

So with these strong caveats regarding model performance in mind, we now attempt to use soundings from a model simulation to illustrate in a broad sense what processes may be at work in the SJ region to allow high momentum air to descend to the surface, inland. The two profiles in Fig. 2b are taken from a good broadscale simulation of Ulli (from the ECMWF 16 km resolution model, i.e. HRES, operational at the time), and span the region of the strongest surface gusts, believed to be SJ-related. Sounding locations are shown with small circles on Fig. 10b. First note that according to discussion in Section 3.3.3 these are correctly located, relative to the mean sea level pressure field, for denoting the SJ impact region. Note also that the related frontal fracture region should be characterised by somewhat increasing temperatures moving west to east, which is again as the soundings show (implying that they span a region of cold advection). Moreover, profiles even further west (not shown) indicated even colder low-level air (3.5°C colder at 950 hPa 80 km from the 'west' sounding). Wind directions and temperatures at the surface also match the criteria put forward by Smart and Browning (2014) for distinguishing a SJ from a CJ. And those criteria were for the same case.

The 'west' sounding has a low-level jet of 100 kts at 920 hPa ($\sim$500 m altitude), which is a very plausible source of strong surface gusts. Whilst we have no verifying data in the vertical for Ulli, it is noteworthy that the over-land Doppler radar cross-section for the Xola SJ case in Pinto

and Silva (2010) also showed a substantial jet at very low levels. In this cross-section, speed continued to increase *downwards* to 550 m, the altitude at which beam coverage ended.

Let us consider how momentum from 920 hPa (on the west sounding) might go on to reach the surface. A dry vertical displacement downwards, in the confines of an atmosphere defined by the same sounding, would continue unimpeded, because environmental potential temperature increases during descent. A moist descent, in which precipitation particulate evaporated (as imagery shows) and helped maintain the parcel wet-bulb (and equivalent) potential temperature, would proceed even more freely, that is gaining even more buoyant energy (for descent) en route. Moreover, if as pulsing on satellite imagery shows, and as trajectory considerations imply, any parcels were to project forwards relative to the system, through the region of cold advection towards the environment characterised by the blue (east) sounding, buoyant energy for descent would be even greater still, because the environment ahead is warmer still. And this horizontal environmental temperature gradient will be retained not just over the ocean but also as the cyclonic system crosses land. In constructing the above arguments, we are alluding to the release of 'DCAPE', or 'downdraught convective available potential energy'. Strictly speaking DSCAPE, relating to downdraught slantwise convection, is the relevant quantity, but in the limit of no vertical wind shear DCAPE = DSCAPE, and on the soundings shown vertical shear is small. So we have a plausible mechanism, based on model sounding data and observational evidence, for momentum and associated strong gusts to propagate downwards to the surface, even inland. One can argue about sounding details, such as the unrealistic looking superadiabat below 930 hPa on the 'west' sounding, which may reflect an inability of the convection scheme to 'keep up' with dynamics related adjustments to airmass temperature, though this is not sufficient of itself to invalidate the above discussion. A key feature seems to be the lower potential temperature around 925 hPa, where the low-level jet is. One can hypothesise that melting (upstream) may have had a role to play in its generation.

It should be reiterated here that results from different models/cases regarding SJs in the lower troposphere in the literature have shown a lack of consistency, and indeed in many the relevant boundary layer processes were 'left to be uncovered by future work'. Although the picture portrayed on soundings in Fig. 2b is structurally similar to that seen for two other cyclonic windstorms in the 2014/15 winter (also in HRES), it does differ markedly from the extreme subsided inversion seen on some simulated SJ soundings for October87 shown in Clark et al. (2005). That was of course another case, and used a very different model from over a decade ago. Clearly question marks continue to surround the repeatability of model SJ simulations, and the processes for generating high gusts inland, though we believe that the low-level release of 'downward instability' in a locally favourable environment, as just discussed, constitutes a very plausible mechanism that is not inconsistent with other publications.

### 3.4. *Cold conveyor belt jet (CJ)*

*3.4.1. Transition to CJ.* As in Clark et al. (2005) and other studies, the CJ starts out behind the bent back front, beneath the cloud head, on the northwestern flank of the cyclone (phase 5 in Fig. 1b). It can coexist with the SJ (if there is one) for a short period but then, as the cloud head begins to encircle the low as described above, the CJ effectively expands to replace the SJ. It grows rapidly to possess lateral dimensions that are usually very much greater than those of the SJ. Fig. 4a shows a 'classical' CJ example for Daria, in which the swathe is about 500 km wide.

Parton et al. (2009) identify what might be termed an 'elevated sting jet' over England that did not correspond with rapid intensification of the parent cyclone Jeanette, and this might seem to be at odds with our definitions. We would however place this case in the CJ category, given that the CJ was present beneath, at the surface. Meanwhile dropsonde observations near to windstorm Friedhelm, in December 2012, as discussed in Baker et al. (2013) and Vaughan et al. (2014), seem to have an elevated SJ structure, probably with a CJ beneath. This interpretation also finds some support in model trajectory analysis by Martinez-Alvarado et al. (2014). Indeed operational synoptic charts for both these cases, at the requisite times, most closely resemble stage 6 on Fig. 1b. It thus seems likely that the disappearance of any SJ phase at the surface may relate to the advance, *underneath*, of the CJ flow. This picture conforms also with the satellite imagery sequences discussed above in Section 3.3.4. The extensive low-level cloud that advances is probably convective cumulus/stratocumulus, in an upper portion of the CJ airstream, and it is not unreasonable to assume that it will be overlain, at least for a time, by remnants of the SJ, which no longer has sufficient downward momentum to impact upon the surface (unless, as in the Parton case, insolation-driven convective overturning is sufficiently vigorous to tap into these remnants).

*3.4.2. Stability.* The CJ resides in a polar airmass that has, to some extent, moved towards the equator. In so doing such airmasses tend to encounter higher SSTs and are as a result often destabilised from below, with upward

fluxes of heat (and moisture) resulting. So CJs over the ocean have stability characteristics that are intrinsically very conducive to downward momentum propagation from the boundary layer top. There are also temporal changes in the nominal boundary layer top during the CJ phase. In the very early stages, when the CJ starts out beneath the cloud head (phase 5 on Fig. 1b), there will be very strong thermal gradients in the vicinity, related to the bent back front and a frontal surface in the vertical that slopes out from the low centre. Thermal wind considerations imply strong vertical wind shear here, with maximum winds potentially not far from the surface. Note that this is the only time that we see noteworthy winds *left* of the cyclone track on Fig. 1a (albeit temporarily). As the cyclone continues to evolve it expands, as does the CJ zone. Thermal gradients around the cyclone lessen, vertical wind shear reduces accordingly, and strong winds extend up to higher levels. So the effective boundary layer depth grows. We then arrive at phase 6 on Fig. 1b, denoted by a black dot (signifying, accordingly, a 'barotropic low'). Strong gusts are possible throughout the CJ phase, but over the ocean at least these can evidently be sourced from higher and higher levels as the cyclone evolves. These over-ocean CJ characteristics apply also to coastal regions with onshore flow. In these two geographical regions, the difference between SJ and CJ gusts may not be that great, because the environments are both conducive to downward momentum propagation, albeit for somewhat different reasons.

Inland the picture for CJ gusts is much more complex. Whilst SST does not readily harmonise with airmass temperature, the land temperature often does, so over land there is often no clear surface-based heat source with which to destabilise. Indeed any net radiative cooling over land will reduce air temperature and stabilise the airmass further. Such conditions naturally prevail at night and when solar elevation is low, and so at such times CJ gusts are usually much lower inland than near windward coasts. At other times however insolation may elevate land temperatures sufficiently to destabilise. In turn, this naturally also depends on time of year and latitude. Cloud cover is clearly also important – CJ airmasses do tend to possess cloud free areas (away from the cloud head). So for example if the CJ is present over land in the early afternoon (local solar time), if we are beyond the cloud head region, and if solar elevation is not too low, gusts inland can be much stronger than they would have been at night. The profile in Fig. 2c, from Crawley in southeast England (location shown on Fig. 4a), was within the CJ zone of Daria, and supports the above. The sonde was released after sunset, between 17 and 18 UTC, and there is clearly a shallow stable layer near the surface, due to nocturnal cooling, to reduce gust magnitude. On the previous sounding, 6 hours earlier (not shown) this stable layer is missing; instead a dry adiabat extends upwards from the surface, probably because of heating of the ground by insolation. Nonetheless even on the late afternoon sounding shown the potential temperature in the lowest 100 hPa or so generally increases less with height than it does on the WJ sounding in Fig. 2a, and accordingly, it seems, the winds in that layer decrease downwards at a slightly lower rate for the CJ case.

The more marked along-flow reduction in CJ gust strength seen inland for Renate (Fig. 4c) than for Daria (Fig. 4a) can be explained by the above insolation-related arguments. Conversely For Ulla, on Fig. 3, whilst the gusts are *generally* greater in the CJ zone than in the WJ zone, the maximum CJ gust (50 kts) was actually less than the maximum WJ gust (55 kts), due in part to time of day and an absence of marked convective activity in the CJ zone (see rainfall trace).

When analysing cyclone simulations within projects such as IMILAST, complications related to insolation need to be borne in mind. Metrics such as 850 hPa wind speed, used by some as a measure of storm intensity, will not reflect this effect, even if the mean sea level pressure field and other aspects are well represented.

Observational data for Friedhelm in Vaughan et al. (2014) highlight what can happen in the over-land case if there *is* significant inland propagation of vigorous marine-based convection. Should this occur (perhaps via the support of broadscale forced ascent) then vertical transfer of momentum associated with the convection (and indeed with evaporation) can accordingly help elevate inland gusts at the surface even when insolation is not really a factor. Vaughan et al. also present convincing evidence that CJ downward momentum transfer prevails in the gaps between precipitating cells, leading to higher surface gusts here. They reported that the average difference over land, for Friedhelm, between gusts measured in convective precipitation and gusts measured in dry (gap) regions was 3 kts (in extremis it reached 10 kts). From a process perspective such variability is analogous to the SJ, wherein gusts are elevated just downstream of gap(s)/furrow(s) in the cloud head tip. A key difference however concerns the direction of downward momentum transfer relative to the parent cloud feature: for the CJ this is essentially vertical relative to convective cells, whereas for the SJ pulses it is slantwise (advancing forward) relative to the cloud head tip. It should also be stressed that in spite of this local augmentation gust magnitude for Friedhelm was typically only about 60 kts, whereas for synoptically-similar storm Ulli gusts over land were about 80 kts. This was simply because Ulli hit the same parts of Scotland slightly earlier in its life cycle (about phase 5 = SJ on Fig. 1b, compared to phase 6 = CJ only for Friedhelm). Indeed the impact of Friedhelm, in terms of damage caused, was very probably much less than it was for Ulli. The reasons are twofold. Firstly the damage

caused by the wind tends to vary with the cube of the speed (e.g. Lamb, 1991), or even speed raised to a power higher than 3 (Prahl et al., 2015). Secondly, damage thresholds, related for example to building regulations, would have been much more readily breached by Ulli's gusts (which probably relates to the aforementioned Prahl et al. result).

*3.4.3. Isobars, curvature and system velocity*. From an isobaric perspective CJ zones exhibit strong gradients, but also marked curvature, which tends to reduce strength markedly below geostrophic levels through the gradient wind effect. However, an important additional consideration here is that it is not strictly curvature on a snapshot pressure chart that is relevant, but rather the curvature of the air parcel trajectory. This brings system velocity into play. The faster a cyclone moves the greater will be the cyclonic curvature of low-level trajectories left of track, and, critically, the less will be the cyclonic curvature of trajectories right of track. So for a given isobaric spacing/gradient wind the faster a low is moving the stronger will be the near-surface winds to the right of the track (in the CJ zone). This may help explain why many high impact CJ cases are associated with cyclones that continue to move quite rapidly around phase 6 on Fig. 1a and b; Daria (Fig. 4a) is a case in point, as highlighted by McCallum (1990). The reduction in spot spacing on Fig. 1a signifies that normally cyclones do slow down around the time of maximum depth: 80% of the ISD cyclones did this. From a dynamical standpoint height contours are becoming increasingly 'stacked' as the cyclone approaches phase 6. This is synonymous in the first instance with evolution towards a more barotropic state, as discussed above. In turn, this necessitates a reduction in upper level steering flow over the cyclone centre, hence the deceleration. So a fruitful area for future study might be determining what dynamical ingredients help a seemingly mature cyclone to retain a sizeable system velocity.

Figure 1 also shows the cyclone track curving to the left, as the system decelerates – in the ISD 67% of cyclone tracks curve to the left, whilst the proportion that curve in this way *and* decelerate is 57%. In a set of all strong cyclones the percentages would probably be much higher; forecasting experience, and track maps such as those in Martinez-Alvarado et al. (2012) show such behaviour to be commonplace. Indeed given the geographical layout of Western Europe, this is probably the main reason why many CJ windstorms miss the main population centres. They give instead just a glancing blow to exposed northwestern coastal regions, and indeed lose impetus during deceleration as the curvature of low-level trajectories has to simultaneously increase. Due to only minor impacts over land such systems would not have been included in the ISD.

*3.4.4. Decay*. The areal extent of the CJ zone often grows as the cyclone grows in size (for Ulli for example the diameter of the largest closed isobar grew from 400 km around the time of maximum depth to about 1000 km 18 hours later). Ultimately however the CJ dies, around stage 7 on Fig. 1. This is due to the aforementioned impact of the low slowing down, combined with a general reduction in geostrophic gradients as it also fills, through friction and through the absence of other counteracting dynamical drivers. Frontal features become weak or non-existent (Fig. 1b), as simple kinematics lead to the increasing interleaving of cloudy and clear zones (sometimes denoted by fragmenting cloud spirals on imagery). The slow decay and ultimate disappearance of the CJ zone are signified with a sloping bar on Fig. 1c, whilst the transient increase in areal extent is denoted by the shape of the CJ footprint on Fig. 1a.

So how common is a damaging CJ? It appears to be much more common than the SJ, and evidence from cases studied suggests that it is also more common than a damaging WJ, at least over Europe. In the ISD, the frequencies of probable WJ, SJ and CJ cases were 10, 9 and 20, respectively. These relative frequencies may relate in part to Europe being the cyclone 'graveyard', where warm sectors have often lost their identity. Almost every deep cyclone will have a CJ phase of sorts associated, but at the same time a lot of these do not have a major impact over land. Note also that Table 1 shows cyclones pre-selected for having caused significant impacts, and so the frequency of phenomena that it shows will not be indicative for all cyclones, but will be heavily weighted towards those exhibiting the more extreme phenomena over land (SJ then CJ). A further complication is that the CJ footprint generally covers a much greater area than the SJ footprint (Fig. 1a), meaning that it is more likely to be sampled by conventional observations, though if a SJ hits forested and/or populated areas the impacts are usually substantial, and it is not likely to go unreported.

### 3.5. *Confidence in windstorm classification*

Having described the key characteristics of each windstorm zone in the preceding subsections we can now remark on how 'confidence levels' were allocated to the windstorm assignations on Table 1, using the example of Herta. This storm was categorised as '(S) C'; bracketing means confidence levels of 50–90% (here for the SJ), unbracketed means >90% (here for the CJ). So why was confidence not >90% for the SJ? Evidence from surface observations and from synoptic charts presented in Young (1990) convincingly suggested that a localised SJ was present, over and west of Paris for example. However, several satellite data outages, one of 4 hours duration, prevented unequivocal association of the strong gusts with the tip of the cloud head.

Also because the gusts peaked in the middle of the day the possibility that these were all attributable to a CJ could not be ruled out, because insolation-driven destabilisation could have enhanced the downward momentum transport. For the other bracketed cases there were also question marks, though reasons varied from case to case.

### 3.6. *Additional considerations*

Close scrutiny of many synoptic charts, and indeed some descriptions of old windstorm cases in Lamb (1991), can suggest events that at first sight do not fit into the Fig. 1 framework especially well. One such example is the strong and relatively straight flow that sometimes occurs ahead of an occlusion belonging to a cyclone that has slowed down markedly, perhaps as it approaches a block in winter. Depending on airmass temperatures and frontal orientation such a flow may have characteristics similar to the WJ or CJ cases, and is thus probably best viewed accordingly. In both instances, however very strong gusts would likely be restricted to exposed coastal sites, because a destabilisation mechanism would be lacking inland, partly because of frontal cloud.

A more significant factor in windstorm enhancement is probably topographic forcing, for example topographic channelling or steering when the geostrophic flow is suitably aligned. In some such cases, a low frontal or anticyclonic inversion may actually enhance the 'squeeze' and elevate mean and gust speeds. There are many documented examples, such as the northerly Mistral in southern France, and the southeasterly Kosava wind in eastern Serbia. Lamb (1991) details some others. It is not possible to encapsulate these phenomena within a cyclone-related view of windstorms as shown in Fig. 1, though forecasters and windstorm analysts have to be aware.

Finally, individual cyclones can sometimes also have additional cyclonic features embedded, which can distort the picture away from that shown in Fig. 1, at least temporarily. One example was the meso-low found within the larger circulation of Xaver (Hewson et al., 2014).

## 4. Re-analyses and windstorms

Having laid out our conceptual picture of the structure of extreme cyclones, and of the footprints of damage left by the extreme winds that are associated, we now go on to assess the degree to which models of different resolution, and in particular the ERA-I re-analysis, can correctly replicate those cyclones. This helps provide an introductory framework for IMILAST and other cyclone studies, for which ERA-I or indeed other model output, such as low-resolution climate runs, provide the input data.

The approach here has two components. Firstly, all 22 ISD storms are referenced in an exercise in which the trend over time of mean sea level pressure at the cyclonic centre is the main metric. It would have been nice to use comprehensive wind gust data for all these storms for validation purposes too, though that is problematic due to observing and reporting practices being inhomogeneous in space and time, to inhomogeneous data density, and above all to a paucity of data over the ocean. Whilst Section 3 focussed more on winds over land, here the aim is to assess ERA-I's ability to handle the different cyclone life-cycle components so there is focus also on marine environments, notably the North Atlantic. The second component is complementary, and involves detailed study for one case, cyclone Ulli, of several metrics including wind gusts. This windstorm was chosen because it occurred over an area and at a time when (1) there were extreme gusts with evidence of a SJ, (2) observation density was quite high and (3) operational runs at many different spatial resolutions (from 1.5 to 80 km) were available for comparison. The case is also relatively 'standard' in two respects. Firstly, it seems to fit the cyclone conceptual model in Fig. 1 well if one imagines the footprints being relocated, and reduced somewhat in areal extent. Secondly, in terms of cyclone size, Ulli seems to be mid-range.

It has long been appreciated that low-resolution models cannot capture important windstorm details. At one level this is basic meteorology: take a storm like Renate, with a closed isobar of 150 km diameter, and a SJ footprint 40 km wide, and try to represent at 80 km resolution, and there will inevitably be difficulties. At another level though the problem is more involved, in particular with regard to the SJ phenomena, which Clark et al. (2005) and others have shown intrinsically requires high horizontal and vertical resolution to represent. Simulating the process of slantwise convection, particularly in models with parameterised convection, is a related complication. Indeed Shutts (1990) pointed out that upward slantwise convective mass transfer may be a key ingredient helping to deepen cyclones such as October87 which have an extensive cloud head. It is in the cloud head that slantwise convection is considered to commonly take place (recall also that the more focussed downward-oriented component of this was discussed in conjunction with the SJ phenomenon in Section 3.3.5). These resolution-related issues that can lead to under-deepening can also be compounded within ERA-I by the way in which data assimilation works. Firstly, the length scale at which assimilation is performed is about double that at which the model runs, which naturally further reduces the resolvability of fine resolution features. And secondly, the covariances that effectively determine whether or not observational data is accepted are a function of geographical location only. So should the background forecast first guess fields that

feed the assimilation exhibit under-deepening of a frontal wave system (say), because of a lack of resolution and/or poorly resolved physics, any good observations valid at the next analysis time, situated close to where the error is, that could have put the model back on track, can effectively then be given low weight or even rejected. A manual analyst would have a clear advantage in such a situation, because they would understand the dynamically active nature of the situation (perhaps with extra clues from imagery). They could infer that pressure reports that are a long way below background, say, are much more likely to be correct then than if the synoptic setting had been a large anticyclone. As far as ERA-I assimilation covariances are concerned, anticyclonic and developmental cyclonic scenarios are indistinguishable.

Many published case studies using the Met Office Unified Model have suggested that it is capable of replicating the SJ if run at sufficiently high horizontal and vertical resolution. Specific sting jet runs with the ECMWF operational IFS (integrated forecast system) model have not yet been performed, to the authors' knowledge, although evidence to be presented below, for the model version operational in January 2012, suggests that gust representation – the user-critical aspect – compares very favourably with the Unified Model, at least when spatial resolution is similar. In turn, this provides some evidence that process representation and gust parameterisation were working satisfactorily in the ECMWF model formulation then in use. It should however be noted here that ERA-I is based on a rather different, older ECMWF model version, that was operational in 2006.

### 4.1. *ISD storms*

In this subsection we compare two manually-generated datasets, the 'definitive' 6-hourly ISD track dataset, whose derivation was described in Section 1 (BESTTRK), and the ERA-I equivalent of this (ERATRK). To derive ERATRK, mean sea level pressure fields from ERA-I were plotted at full resolution ($\sim$80 km) at 6-hour intervals for the duration of each cyclone as defined in BESTTRK. Overlaid on this were 850 hPa temperature fields, to provide a means of cross-referencing fronts drawn on the synoptic charts used as input to BESTTRK, recognising that frontal wave stages 1 and 2 on Fig. 1b were important starting points for many cyclones. These plots were manually examined to determine which cyclonic centres corresponded to the BESTTRK cyclones, and then mean sea level pressure at these centres was recorded every 6 hours, along with position, to make up ERATRK. For the vast majority of the time cyclone association between the two datasets was unambiguous, though in a few instances early in the life cycles it was problematic. In these problematic cases, BESTTRK was probably more accurate, due to the fact that the chief forecaster preparing the related synoptic charts performs real-time quality control on SYNOP observations (notably for ships), and uses imagery interpretation, background fields from operational models run at high resolution (e.g. 12 km), and hourly data, all of which are lacking in the assimilation used in ERA-Interim. We also applied one additional 'reality check' on the Met Office charts that had been the basis of BESTTRK. For all the ISD cases, we compared with equivalent operational charts prepared by the Deutscher Wetterdienst: the mean difference in cyclone depth was only 0.3 hPa. This turns out to be very small in comparison to the ERATRK versus BESTTRK differences discussed below, and so supports our results.

Figure 6 shows how the feature central pressures in ERATRK compared with BESTTRK, by plotting for each cyclone the pressure difference on the y-axis, as a function of time in hours on the x-axis. Values on the x-axis have been normalised to put the time of maximum depth (in BESTTRK) at $x = 0$ (vertical grey line).

Whilst there is considerable variability amongst the cases, some common features stand out. For example, the cyclones in ERA-Interim are on average too shallow by 4 hPa when at their deepest. In the deepening phase, which is essentially left of $x = 0$, there is systematic under-representation of depth, by 1–3 hPa on average, whereas in the filling phase, right of $x = 0$, the biases are minor. More striking is the error at the end of the 6-hour period of most rapid deepening (in BESTTRK, pink circles) which has a mean of 5.3 hPa, and in 30% of cases is $\geq$8 hPa. The largest difference, a remarkable 17 hPa, is for Lothar. This corresponds to a time when Lothar was situated in a data rich area close to Paris, and was giving rise to exceptionally damaging gusts of order 90 kts. Klaus has the equal second largest difference; fortunately this was at a time when it was over the Atlantic, far from land. For both Lothar and Klaus, most if not all operational models, from different centres, which have much better (higher) resolution than ERA-Interim, provided significant under-predictions of rapid deepening, implying a general modelling difficulty for these cases.

The trace for Martin is also interesting. After showing insufficient depth, by up to 9 hPa, in the deepening phase (over the Atlantic) the feature becomes consistently too deep over land, albeit by small amounts. This was a relatively large cyclone and it seems possible that latent energy, such as latent heat, that should have been expunged over the ocean was perhaps released over land instead, with observation assimilation perhaps fighting against a related tendency in model background fields for the cyclone to be over-deep there, but not quite succeeding.

Early in the life cycles of Gordon and Lili the central pressure in ERATRK is evidently far too high, but it improves later. This evolution is a symptom of the ET process;

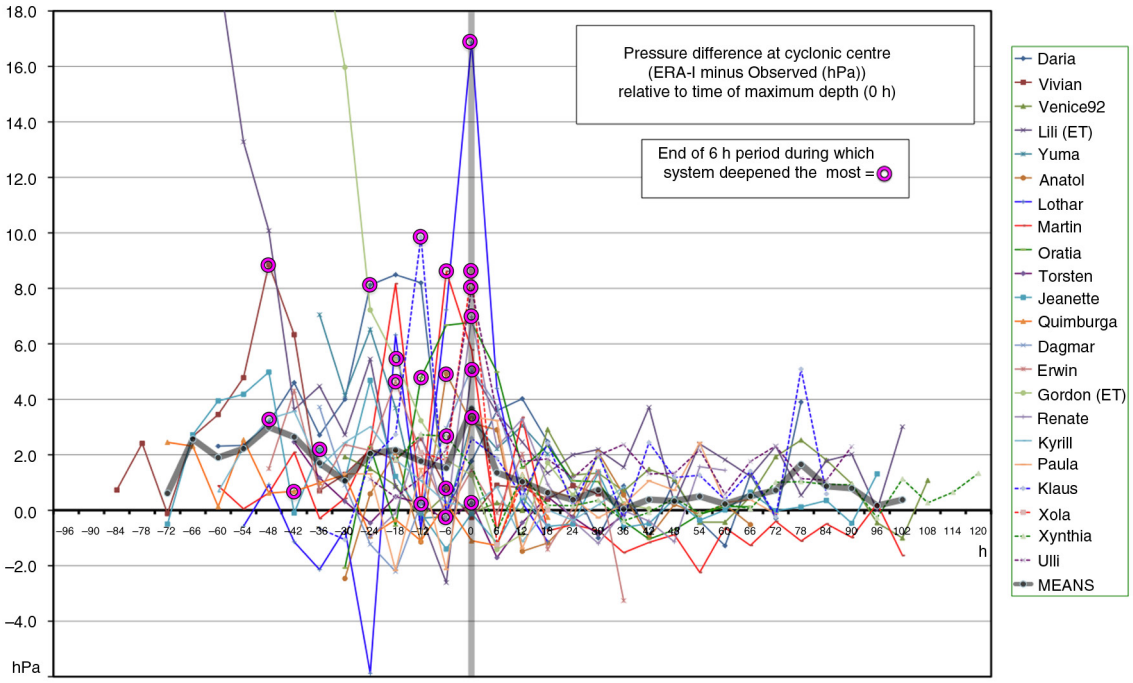


*Fig. 6.* Differences between cyclone central pressure in ERA-Interim (ERATRK) and in the best-track dataset (BESTTRK), in hPa, for each IMILAST windstorm (see legend). The x-axis shows hours relative to the (best-track) time of maximum depth for each cyclone. The thick grey line denotes mean behaviour (plotted only when at least three cyclones contributed). Pink rings denote the end of the 6-hour period during which the cyclone deepened the most (BESTTRK). For the two extra-tropical transition cases (ET in legend) only the extra-tropical phase was considered when identifying the times of maximum depth and maximum deepening.

the early discrepancies denote the inability of the re-analysis to handle the tight cores of tropical cyclones; later on, after transition, when the cores are much broader, the representation is rather better.

As the ability of ERA-I to replicate windstorms is of particular interest, the fact that cyclones are systematically not deep enough is clearly a concern. This concern is heightened by the discrepancies being larger at the end of the period of most rapid deepening, because this is the period during which the most damaging phenomena, the SJ and CJ, tend to develop (recall the blue markers on Fig. 1a–c).

To further illustrate, we show on Fig. 7, for each cyclone, the BESTTRK and ERATRK deepening rates at the time when the BESTTRK deepening was the greatest. In 68% of cases the deepening rate shortfall in BESTTRK is 25% or more; in 23% of cases it is 50% or more. Some of the smallest cyclones appear to have the largest relative errors (e.g. Lothar, Renate, Xola), which is unsurprising given the resolution constraint. Interestingly the largest absolute deepening rates all occurred in December 1999 (Lothar, Martin and Anatol).

For only one cyclone is the deepening rate in ERATRK greater than in BESTTRK. This was for Gordon, at the time of ET. Only after this transition event would ERA-I have a chance of accurately representing the cyclone's core, and because of this perhaps there is a more noteworthy downward jump in pressure in ERATRK. It appears that this issue was compounded by a misplacement error of 300 km for Gordon in ERATRK just before transition. Within the re-analysis, this may signify that not being able to capture a tropical cyclone's core may adversely affect the representation of that cyclone's movement, which in turn, via assimilation of other data for a later time, could amplify the core pressure error.

A brief remark should be made regarding error bars related to Figs. 6 and 7. Whilst strident efforts were made to reduce errors in BESTTRK, there remains a clear dependence on data coverage, amongst other things. Accordingly we infer a standard error bar on BESTTRK central pressure estimates of 1–2 hPa in marine areas and 0.5–1 hPa over land. These values are sufficiently small to not jeopardise in any way the general conclusions that have been drawn. Another issue arises because of temporal discretisation. Only standard synoptic hours (00, 06, 12, 18 UTC) have been used, so it is likely that the true maximum 6-hour deepening was greater than shown, in both ERATRK and BESTTRK, for most cases. By way of example one of the

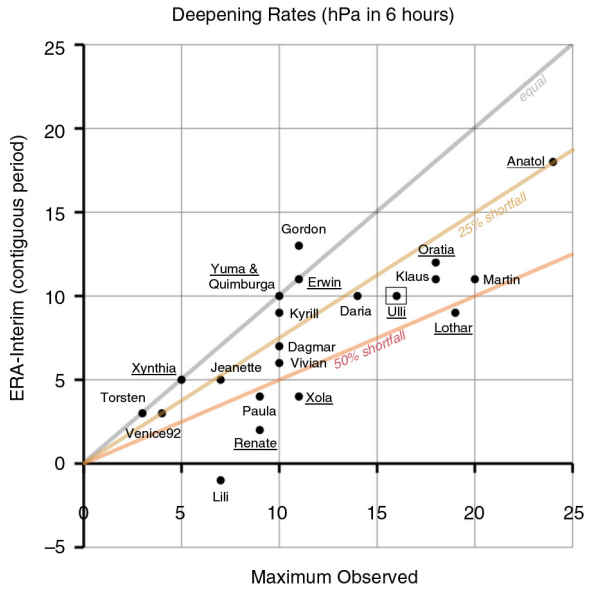


*Fig. 7.* Maximum observed 6-hour deepening (=change in central pressure) for the ISD cyclones, in hPa, compared to the 6-hour cyclone deepening shown by ERA-Interim over a contiguous period. Diagonal lines are shown as a guide, signifying the degree of shortfall in ERA-Interim. Underlining of storm names denotes that the storm was believed to have a sting jet footprint associated *over land* (as on Table 1). A box highlights the Ulli cyclone discussed in Section 4.

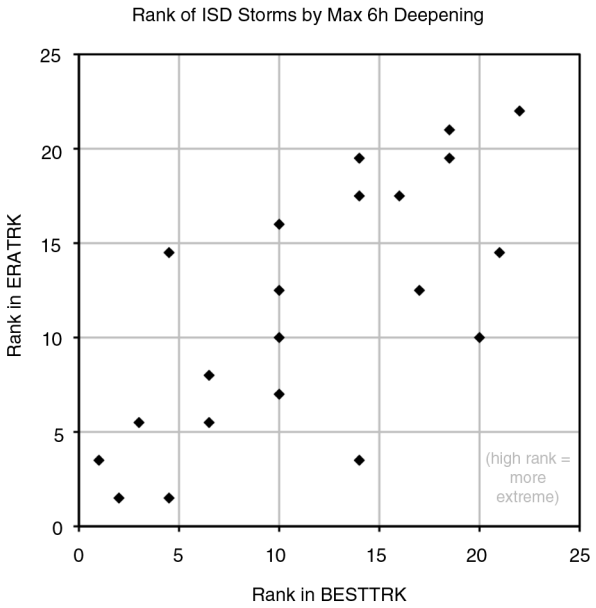


*Fig. 8.* Relative ranks of the 22 ISD storms in BESTTRK (x-axis) and ERATRK (y-axis) using maximum 6-hour deepening during each cyclone's life-cycle as the metric. Higher ranks denote more extreme deepening. The tropical phases for the two ET cases were discounted.

most extreme cyclones, Xola, seems to have deepened in reality by as much as 20 hPa in 6 hours (reaching a depth of 969 hPa or lower around 04 UTC – based on data in Pinto and Silva, 2010). This is almost twice the value shown on Fig. 7, and taking other relevant aspects into account too we suspect that ERA-I performance was actually worse for this case than it appears to be on Fig. 7.

It is not uncommon for studies on climate change to recognise that climate model resolution is a limiting factor and to then accordingly apply/infer an adjustment factor, to in effect re-calibrate the model output to match up with a presumed truth. Such adjustments may be regression-based or quantile-based, though a common underlying principle in both is that storm severity ranking is consistent between model and reality. With our data, we can in principle test this, by comparing ERATRK with BESTTRK. The main difficulty is determining what metric to use to represent storm severity. For this, we have again chosen the maximum 6-hour deepening. So does the rank of real storms, based on this metric, match the rank of ERA-I storms? Figure 8 shows that whilst there is some rank correlation in the correct sense, the scatter is considerable. Some of the most extreme storms are not classed as such in ERA-I. This implies that one should be very cautious about relying on re-calibration techniques. System size is again probably the main complication, with larger systems being much better represented in ERA-I. Whilst results in Martinez-Alvarado et al. (2012) might suggest that there would be ways of addressing this, by identifying which systems in ERA-I have the propensity to generate SJs even if the SJs themselves were not represented, at the same time it should be noted that their approach has an inbuilt scale-dependence (discussed further in Section 4.3). So refining any re-calibration technique to deal differently with small systems would not be at all straightforward. Importantly, for IMILAST and other tracking-related initiatives, Fig. 8 also means that attempts to use a simple model-based metric to de-select the most damaging cyclones from a large set of automatically identified global model cyclone tracks, in re-analyses or climate runs, are likely to fail. For a potential alternative approach, see Deroche et al. (2014).

In this section we have highlighted the fact that ERA-I suffers from discrepancies that systematically weaken cyclones when they are at their most active, and we have inferred that the representation of extreme windstorms suffers as a result. In the following section, a single case is used to illustrate more clearly the potential impact on gradients and surface winds, and to highlight what resolution might be needed to overcome this. Note that the chosen cyclone, Ulli, is fairly close to being mid-range on Fig. 7, implying that the results to be presented should have some general applicability.

### 4.2. Windstorm Ulli

Smart and Browning (2014) performed high-resolution simulations for the Ulli case with the WRF (Weather Research and Forecasting) model. They found some evidence of a SJ in this simulation but indicated that the CJ was stronger, and that the maximum gusts at Malin Head, a very exposed site on the north coast of Ireland, were probably attributable to the CJ. We do not disagree that the cyclone may have had a substantial CJ associated, but would contend that it probably had a more pronounced SJ than their simulations show, and that this was the main driver of the exceptional gusts measured across at least the central belt of Scotland. Our evidence for this is as follows: the degree of inland penetration of very strong gusts was substantial (Fig. 9a, maximum gusts at Glasgow and Edinburgh had a return period of order 20 yr), there were evaporating cloud head tips on imagery (Fig. 9c), there were holes/warm topped clouds between these tips, the peak gusts at Islay and Glasgow (the two sites for which we have comprehensive gust records) lay directly in line with one of these (see Fig. 9b and c), and the frontal structure at the requisite time (not shown) was commensurate with phases 4 and 5 on Fig. 1b. In addition, at Glasgow Bishopton the screen temperature fell a further 2°C after the time of maximum gust, unlike Malin Head where Smart and Browning show the strongest gusts to have been in the cold air. Although Smart and Browning's simulated cyclone achieved the right depth, to within 1 hPa, at 06 UTC on 3rd (an hour or so before the strongest gusts hit southern Scotland), the 6-hour deepening up to this time, which was the actual period of maximum 6-hour deepening in BESTTRK, was only 8 hPa, compared to 16 hPa in BESTTRK (Fig. 7). It is conceivable that the lack of extreme deepening in this period, and a higher-than-observed pressure fall in the previous 6 hours, led their simulations to have under-active sting jet activity and/or sting jet activity that occurred too soon.

To illustrate resolution-related difficulties that operational models and ERA-I had in representing Ulli at 06 UTC on 3rd, we compare in Fig. 10a–c mean sea level pressure fields from three simulations: ERA-I (10a), an ECMWF high-resolution forecast (10b) and a Met Office 'UK4' limited area model forecast (10c). These models have horizontal resolutions of 80, 16 and 4km, respectively. Black boxes overlaid near the low centre in each case denote the gridbox size; it is immediately apparent how limiting the 80-km resolution of ERA-I is for representing a windstorm such as this. In Fig. 10d, valid for the same time, we summarise output from these and other models in terms of the minimum central pressure, maximum geostrophic wind and maximum diagnosed gust strength. In all instances gusts are a parametrised quantity, based on Panofsky et al. (1977).

In preparing Fig. 10, we have used only analyses or short-range (3–11 hour) forecasts, working on the principle that at such lead times the output of each model ought to be about as good as it can be. The intention in so doing is to uncover the systematic limitations of the different model configurations, and in particular their resolutions, and to not complicate this picture with forecast sensitivity aspects. Although it also has to be acknowledged that assimilation issues, and (for the 1.5- and 4-km runs) lateral boundary condition issues may have had roles to play too, the picture that emerges is nonetheless a consistent one, with only the runs with a high spatial resolution (less than about 20 km) achieving what might be termed satisfactory forecasts from a user perspective, and with quality dropping off substantially at lower resolution (Fig. 10d).

The main quality issue is the absence of strong gradients in and just upwind of the sting jet region, a result that is clearly illustrated by comparing Fig. 10a and b. Although the low in the UK4 run in Fig. 10c is misplaced somewhat (which is of course critical for forecasts, as discussed in Fox et al., 2012) this run seems to provide the best simulation overall of the metrics shown. Its output also exhibited clear cloud head filaments, and gaps between those filaments (not shown) that seem to tally with the very strong gusts. Note also how on Fig. 10c the heaviest precipitation is just upwind of the strongest gusts (red and pink shading), but that those gusts are at the same time focussed on a gap where the precipitation rate is zero. This is all consistent with the SJ morphology discussed in various papers and alluded to above – most notably the rapid descent of an airstream from within an active cloud head region. It is also consistent with observations: there were cloud gaps in reality (green arrows on Fig. 9c), plan-view radar data showed precipitation gaps coinciding perfectly with these (not shown), and the peak gusts coincided with these too.

It was particularly encouraging to see that UK4 runs could generate filaments in the cloud head tip region of about the right dimensions, and gaps in the low cloud region just downwind. To the authors' knowledge such features have not been seen before in published SJ case simulations.

### 4.3. Summary of ERA-I performance

In Section 4, the intrinsic resolution-related limitations of ERA-I (and by implication other low-resolution models) have been documented for many European windstorm cases. Such weaknesses have been highlighted qualitatively before; see for example discussion in Martinez-Alvarado et al. (2012) and Roberts et al. (2014). The new result here is the quantitative treatment. The largest errors tend to occur during the period of most rapid deepening, and this may relate to the fact that instability to (upward)

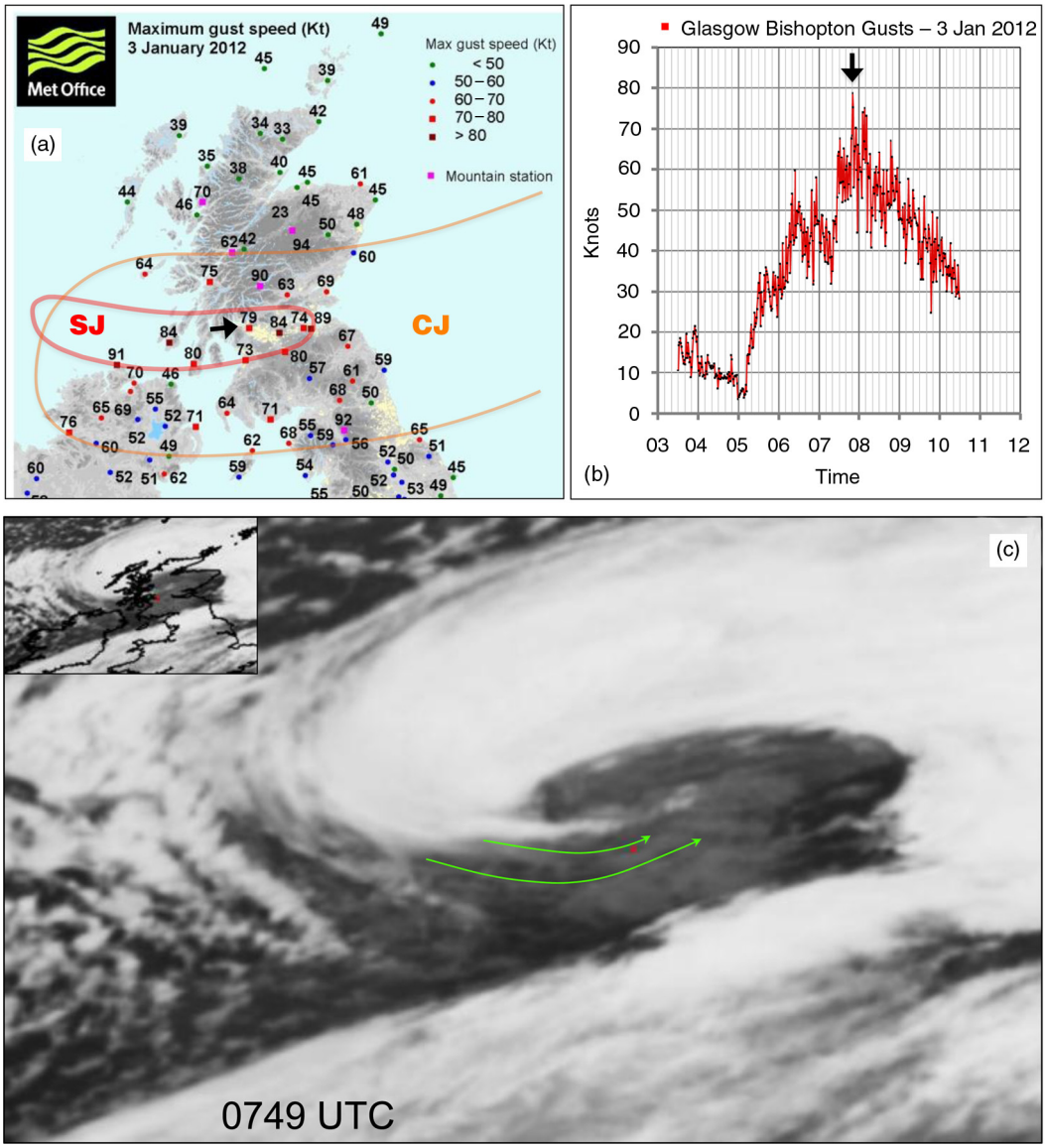


*Fig. 9.* Observational data for cyclone Ulli that hit Scotland on 3 January 2012 (Table 1). Panel (a) shows maximum reported gusts that day in kts. Orange and red outlines denote the areas of influence of the CJ and SJ, respectively (as on Fig. 1a). These were deduced from surface observations and from signatures on a 5-minute interval satellite image sequence, both of which were cross-referenced with mean sea level pressure, maximum gust, precipitation rate and simulated cloud fields from an operational run of the Met Office's UK4 model with a nominal data time of 21 UTC on 2nd (this run is also represented on Fig. 10c and d). An arrow points to the Glasgow Bishopton site. Panel (b) shows 1 minute maximum gust observations from this site, in kts, between 3 and 12 UTC on 3rd. Panel (c) shows an infra-red image for the time of the maximum gust at Bishopton. Green arrows denote two gaps between cloud head tips/fingers that retained their identities on the image sequence. The northern one is believed to relate to the sting jet maximum gust arrowed on panel (b), the site is shown (nearby) with a red dot. Note that parallax errors exist due to the remoteness of the subsatellite point (0°N, 7.5°E). The inset is a duplicate with coasts added. (Observations on panels a and b are reproduced with permission from the Met Office).

slantwise convection, if it exists in the model runs, cannot be released, and so the associated slantwise mass transfer, which contributes to the deepening, is also underestimated. In a similar way, the more focussed release of downdraught slantwise convective instability, that itself is the probable source of the SJ, is also being underestimated or is absent.

For one well-observed cyclone case that showed strong evidence of a SJ, the shortfalls in strong wind metrics were extremely large. The maximum geostrophic wind was only about 25% of observed, and the maximum gust 70% of observed. If one assumes, as in Section 3.4.2, that the destructive power of the strongest gusts (a primary

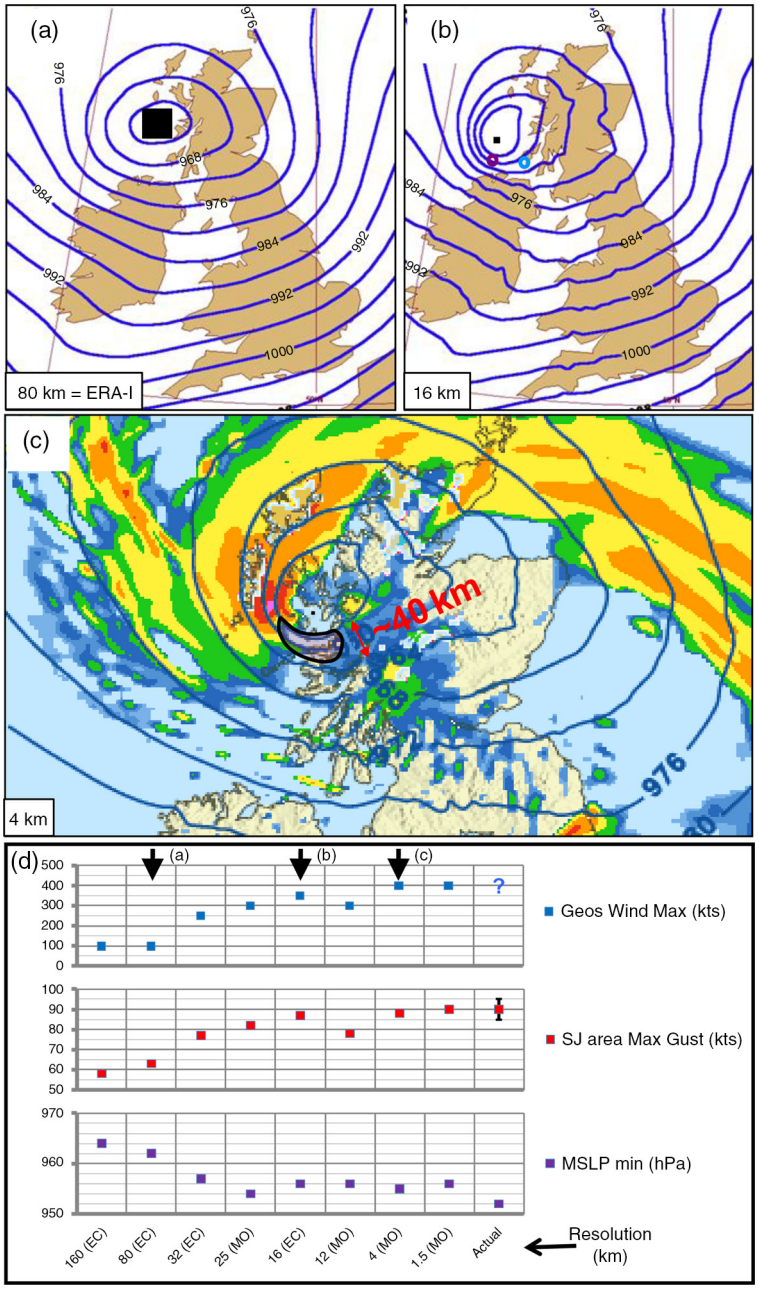


*Fig. 10.* Numerical model representations of IMILAST cyclone Ulli (Table 1) on 3 January 2012. Panels (a) and (b) show, for 06 UTC on 3rd, mean sea level pressure in hPa from, respectively, the ERA-Interim re-analysis (80 km resolution) and the 6-hour ECMWF HRES (high-resolution, 16 km) forecast. Panel (c) shows, for 08 UTC on 3rd, from the Met Office UK4 model run with a nominal data time of 21 UTC on 2nd, mean sea level pressure contours in hPa, precipitation rate in colour (blue, green, yellow, orange, red, pink denote 0.1–1, 1–2, 2–4, 4–8, 8–16, 16–32 mm/hr, respectively; lighter shades with a pale blue outline denote snow) and an 80 kt gust isotach (black). On each of panels (a, b, c) a black box near the cyclone centre shows effective model gridbox size. Coloured rings on (b) denote the locations of model soundings shown in Fig. 2b. Panel (d) compares three windstorm metrics – the cyclone central pressure (hPa, purple), the maximum sting jet gusts (kts, red) and the maximum geostrophic wind (kts, blue), at 06 UTC on 3rd, as represented in various Met Office (MO) and ECMWF (EC) operational forecast runs and re-analyses (labelled below with horizontal resolution given in km). Actual denotes observations. Data sparseness makes measuring the actual maximum geostrophic wind impossible though metric match up with the higher resolution models suggests that it was about 400 kts. The leftmost model is ERA-Interim data extracted at lower resolution (160 km); climatological results in Neu et al. (2013) used input data at this resolution. Arrows highlight the models shown in panels (a,b,c). (Panel c is reproduced with permission from the Met Office).

consideration regarding impacts) varies as the third power (or more) of the speed, then the destructive power of ERA-Interim winds was less than 33% of observed.

Martinez-Alvarado et al. (2012) have usefully highlighted that although discrete SJ trajectories in ERA-I cyclone simulations are absent, their presence in the equivalent situation in the real world can be anticipated by diagnosing slantwise convective instability in analysis fields. However, it should be noted that their selection of extreme cyclones for analysis was based on sorting vorticity values derived at T42 resolution. A simple finite difference derivation of such a value would use grid point winds separated by about 900 km, which is slightly less than the y-dimension of the plot area in Fig. 10a and b. This is evidently far too coarse a grid to capture the tightness of the cyclone core where the SJ was found (Fig. 9a–c), and so their analysis may thus be biased towards selecting out for analysis cyclones that were larger than Ulli, and indeed probably larger than the majority of ISD cyclones in Table 1. So whether or not the presence of a SJ in the ISD cyclones could be usefully anticipated using their techniques on ERA-I is questionable. The fact that our ISD relates to storms that caused impacts over land whilst virtually all their cases were remote from land is probably related.

Though not discussed in detail in this section the WJ and CJ phenomena, by virtue of being larger in areal extent (Fig. 1a), and by virtue of primarily existing at times when cyclone central pressure in ERA-I is relatively accurate (left and right of x = 0 on Fig. 6, for WJ and CJ, respectively) are relatively well represented in ERA-I. For the WJ, note on Fig. 10 how the pressure gradient over England, where the warm sector is and where any WJ would be, is actually much the same in ERA-I (10a) as it is in the overall much better simulation in (10b). However, the *early part* of the CJ phase can be somewhat underestimated in ERA-I. This is because it has less areal extent (Fig. 1a), because it almost overlaps with the SJ if there is one (Fig. 1a and 9a), because it is stronger than later on (Fig. 1c), because it will be more influenced by the aforementioned deepening errors, and because it is closer to the cyclone centre where gradients are poorest (Fig. 10a–c). Due again to resolution limitations one would expect any such shortfall to be most marked for small cyclones. These various findings were included in the final row on Table 2, and are shown pictorially on Fig. 11, which links back to the schematic in Fig. 1c.

So ERA-I clearly has its limitations for representing windstorms. Evidently users must appreciate these limitations, which are most acute for small systems. Lothar is probably the prime example – it was extreme in terms of both economic losses and wind strengths, but was very poorly handled by ERA-I. At the other end of the scale is Kyrill, which according to various estimates in Mitchell-Wallace and Mitchell (2007) and Roberts et al. (2014) lead to economic losses comparable to Lothar, between about 5 and 8 billion Euros. Kyrill was essentially a much larger system, in part because it was embedded in a much stronger broadscale pressure gradient (discussed in Fink et al., 2009), although peak winds were much less than for Lothar. Because of Kyrill's large size ERA-I representation was much better.

## 5. The IMILAST project

### 5.1. *Project overview*

As already highlighted, the WJ, CJ and SJ phenomena associated with mid-latitude cyclones have the propensity to cause considerable damage, and indeed rank as a major cause of natural disasters in the extra-tropics. As a result, stakeholders take great interest in cyclones, and in the possible influences of climate change on their characteristics, such as frequency, intensity, duration and clustering. These stakeholders include the insurance industry, the

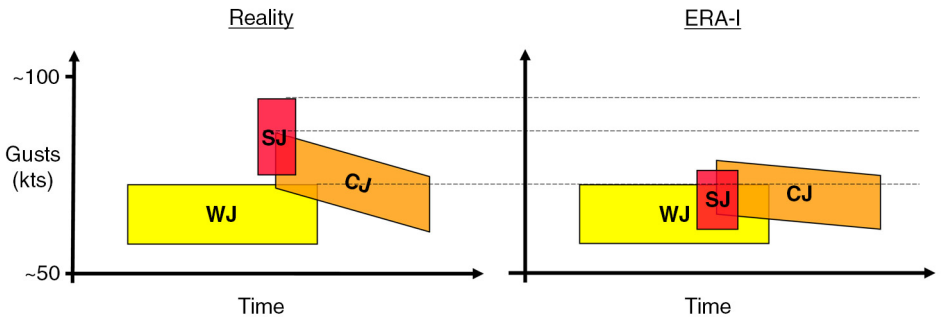


*Fig. 11.* Schematic showing how ERA-Interim's representation of 10 m wind gusts over land during the passage of a cyclonic windstorm (right side) typically compares with observed values (left side). WJ, SJ and CJ are, respectively, the warm jet, sting jet and cold jet phenomena (see Fig. 1).

building industry, and agencies involved in disaster risk reduction. So for such 'customers' there is a clear need to not just document and understand windstorms and investigate how they are represented in models, but also to look at how well automated methods actually perform the task of identification and tracking. For practical reasons, one clearly has to use automated techniques if more than just a few events are being systematically studied.

Historically, it is an unfortunate fact that studies using automated tracking to examine cyclone activity in climate change scenarios have been quite diverse, and have sometimes even shown seemingly contradictory results. Moreover, these different studies were often not comparable since they used different input data, different identification and tracking algorithms, and looked at different regions and different time periods. The scientific information provided therefore was thus not that useful for stakeholders.

Initial attempts to *directly compare* identification and tracking algorithms showed that different methods might provide rather different conclusions and even opposite signs for certain trends (Raible et al., 2008; Ulbrich et al., 2009). To investigate this problem in a consistent way, a few scientists involved in the field initiated the IMILAST project in 2009, with the aim of performing a coordinated intercomparison, using various input datasets (we use the term 'experiment' to describe each intercomparison activity). Soon afterwards others joined the project, and today about 20 groups using more than a dozen different methods take part. Until now four experiments have been performed (see Table 4); the results of two have been published recently (Neu et al., 2013; Ulbrich et al., 2013). More in-depth analysis of experiment 4 and (partly) experiment 3 are published in papers in this special issue.

Experiment 1 used the ERA-I dataset at 1.5° resolution for the period 1989 to 2009 (the full period that was initially available) and aimed to get an overview of the scatter in a range of track-related parameters delivered by different algorithms. Meanwhile experiment 2 aimed to assess the influence that using different algorithms had on what an inferred climate change signal was. The main signal investigated was differences in cyclone density between the end of the 20th century (average 1961–2000) and the end of the 21st century (average 2061–2100). A single set of climate model runs provided the input data – these were the first runs of the ECHAM5/OM1 model. The runs were all based on the 'A1B' emissions scenario. Compared to other IPCC (Intergovernmental Panel on Climate Change) scenarios A1B is mid-range, with emissions peaking around 2050 then declining slowly.

Experiment 3 focusses on the ISD and uses these cases to assess how using different algorithms affects the reproduction of tracks of extreme storms. Clearly this activity has to recognise that ERA-I has imperfections when it comes to representing strong-wind-generating phenomena associated with extreme cyclones, notably the SJ, as we have detailed above.

For the more comprehensive climatological analyses described in this special issue, it was possible to extend the dataset of experiment 1 to encompass 30 yr rather than 20 by adding the period 1979–1989, and this we label experiment 4. For the calculation of tracks, the resolution of 1.5° was retained to ease comparison with the results of experiment 1 (although 0.75° resolution ERA-I data is now publicly available online). The downside of this approach is that lower resolutions are suboptimal as Section 4.2 clearly shows. The leftmost two columns of Fig. 10d give an idea of the likely impact, albeit from just one case.

### 5.2. *The intercomparison strategy*

An intercomparison of the output of different algorithms poses a number of questions from the outset, the main one being what in fact we want to compare. A basic problem is that there is no universally accepted definition of what a 'cyclone' or a 'storm' actually is. Therefore, each research group dealing with cyclones has tended to set up its own definition. During recent decades, many such groups established algorithms in this way and used them to track storms in gridded input fields (Murray and Simmonds, 1991; Hodges, 1995; Serreze, 1995; Blender et al., 1997; Sinclair, 1997; Simmonds et al., 1999; Lionello et al., 2002; Benestad and Chen, 2006; Trigo, 2006; Wernli and Schwierz, 2006;

*Table 4.* IMILAST experiments in the period 2009–2015, in chronological order

| Expt. no. | Input data | Period | Region | No. of methods | Publications |
|---|---|---|---|---|---|
| 1 | Re-analysis, ERA-I, 1.5° resolution | 1989–2009 | NH, SH | 15 | Neu et al. (2013) |
| 2 | Climate model, ECHAM5/OM1, A1B scenario | 1961–2000; 2061–2100 | NH | 11 | Ulbrich et al. (2013) |
| 3 | Re-analysis, ERA-I, 0.75° resolution | Single storms | North Atlantic & Europe | 12 | TELLUS special issue |
| 4 | Re-analysis, ERA-I, 1.5° resolution | 1979–2009 | NH, SH | 14 | TELLUS special issue |

NH denotes northern hemisphere extra-tropics, SH the southern hemisphere extra-tropics.

Akperov et al., 2007; Rudeva and Gulev, 2007; Inatsu, 2009; Hewson and Titley, 2010; Kew et al., 2010; Hanley and Caballero, 2012). They used many methods, starting off with different input parameters like pressure, pressure gradient, vorticity or wind speed, and also using different height levels (surface, 1000 hPa, 850 hPa). Furthermore, parameter thresholds were chosen differently, by specifying for example how strong the pressure gradient of a low pressure system has to be for that system to be considered a 'cyclone' or 'storm', how long a system has to exist to be taken into account, or whether 'closed' pressure contour lines are necessary. These and other choices can be made in light of the specific scientific question(s) being addressed, or alternatively may depend on a personal understanding of what a cyclone is. Because of this one can neither compare algorithms designed for the same purpose, because purposes vary, nor easily adapt algorithms to 'fit' a particular question, because particular aspects of a cyclone may be investigated in different ways.

So for the IMILAST intercomparisons, we were essentially left with two options. We could choose a few methods that addressed a particular issue, with the aim of getting an impression of the methodological uncertainty for that issue. Or we could choose to compare all existing methods as is, independent of their main purposes, to get an overall impression of the disparities that arise because of choice of algorithm (in cyclone density trends, for example). For IMILAST, the latter 'all-embracing' strategy was adopted, since it is more inclusive and reflects the reality that many users (policymakers, insurance industry etc.) are normally confronted with.

From the outset, following discussion amongst participants, it was deemed appropriate to implement standardisation for just two aspects. The first was a threshold on lifetime, that is the number of consecutive time steps that a tracked system needs to exist to be considered a 'cyclone'. An increase or decrease of this threshold obviously leads to a decrease or increase, respectively, in the number of identified cyclones. The threshold of lifetime is a somewhat arbitrary choice, which can be standardised easily between methods, and following discussion we settled on 1 d as the minimum permissible. As a point of reference, we found that for ISD cyclones, as represented in BESTTRK (with the two long-lived transitioning tropical cyclone cases excluded), the mean lifetime was 4.25 d, the minimum 1.25 d (Xola) and the maximum 7 d (Jeanette). Note also that these lifetimes would have been shorter if only centres denoted by a pressure or height minimum had been retained – this would have been equivalent to starting out at stage 3 on Fig. 1.

The second standardisation concerned the elimination of high elevation areas, that is mountains. Some methods include cyclones over high terrain (e.g. higher than 1000 or 1500 m) whilst others do not. This of course leads to a different area being considered and therefore compromises any comparison of total numbers. For examination of geographical distributions, this problem is not so relevant (methods including mountain terrain just show values there whilst others do not) and so the original tracks could be used. For the calculation of area averages, however a second set of track data was computed (for each method) which uniformly eliminated all cyclones over grid points that had an elevation of more than 1500 m in the ERA-I model orography.

Other characteristics, such as system velocity or distance travelled, are much less amenable to standardisation, because algorithms are sometimes built up around these aspects. Moreover such aspects can have a strong relationship with certain cyclone types and we did not want to accidentally exclude what might be important features. Let's say for example that we excluded slow-moving cyclones, to get rid of heat lows, then we might inadvertently remove old Icelandic lows, for example, as they too can move very slowly. And furthermore many other parameters cannot be standardised anyway because they are only used by a few methods (examples are pressure gradient and wind speed).

### 5.3. *Initial results and future directions*

The main results of experiments 1 and 2 are described in Neu et al. (2013) and Ulbrich et al. (2013), respectively. One important result was that findings concerning strong or extreme cyclones – in so far as they are represented in ERA-I or climate runs – are more robust with regard to the choice of algorithm than are findings for all cyclones. Spatial patterns of past and potential future trends were also found to be fairly consistent, despite the fact that different methods identified very different total cyclone numbers. Concerning more technical issues, the most important insight gained was that conclusions from a particular investigation, though they might vary with the algorithm employed, did not seem to cluster according to the cyclone identifying parameter(s) used (e.g. surface pressure, 850 hPa height or low-level vorticity). Differences seemed to depend instead on other methodological aspects, such as threshold setting.

While experiments to date have already provided many results, there is still much to draw out, either from existent data or from further experimentation with different settings. Scientific questions that could be addressed include a more extensive look at climate change signals, and the problem of ET, whereby a tropical cyclone becomes extratropical. Throughout such studies one must always bear in mind how good the input dataset is, however, by referring to case analysis. For example, the Gordon and Lili cases on Fig. 6 usefully suggested that tropical cyclones are not especially well resolved in ERA-I, and clearly this could impact upon any ERA-I based ET analysis.

There are also questions that will probably remain unresolved: the assessment of the overall *quality* of different algorithms has not been and cannot really be an aim of the IMILAST project. The reasons are twofold. Firstly differences in algorithm performance may arise because of the different purposes that underpinned algorithm development, as stated earlier. Secondly there is no universal 'truth' concerning the location and the track of a certain cyclone, partly because of uncertainties arising due to incomplete data coverage, and partly because of the cyclone definition problem. And as we saw in Section 4, different 'levels' of truth exist, be it the BESTTRK dataset we have constructed for the ISD, or the manually constructed ERATRK. BESTTRK might be considered to be the best that we can achieve, but as already highlighted it is completely impractical to construct in any considered way a version for all cyclones over a long period, and very clearly ERA-I (which has the requisit temporal coverage) does not capture some of the cyclones well anyway, for a variety of reasons. So for individual methods the best we can hope to do from the point of view of major storms is to replicate ERATRK, and in this regard at least we may in time be able to provide some useful pointers regarding performance. Let's say for example that one method failed to track most of these storms because it did not allow for systems to move fast enough, then that would not unreasonably register as a disadvantage of that method.

## 6. Summary and discussion

This paper aimed to give a comprehensive overview of the characteristics of cyclonic windstorms that affect the North Atlantic and Europe. In part, this was to provide a framework in which the results of IMILAST could be viewed. A second aim was to show how well model analyses (and very short-range forecasts) represent the key windstorm characteristics, and special focus was placed on the ERA-I re-analyses as these provided a key input to the IMILAST project, and are also used widely elsewhere. We then briefly described IMILAST – its aims, its structure and its results to date – and looked forward to future work within its framework.

The description of cyclonic windstorms and the damage 'footprints' that they can leave behind is comprehensive and provides many new scientific results. Our malleable conceptual model (Fig. 1 and Table 2) has been developed over many years, and is based on a synthesis of the structures seen in both old (published) and new case studies of cyclones. For this paper, almost all of these cyclones were revisited, using many types of observational data (notably imagery with a high temporal resolution, and standard hourly surface observations) and synoptic charts (manual and automated), and for the older published work we placed special emphasis on looking for phenomena that the authors at the time would have been unaware of, such as the SJ.

Windstorms have been broken down into three distinct causal classes, the WJ, the SJ and the CJ. Whilst this is not new, what are new are our descriptions of (1) the typical sizes of the footprints left behind – the SJ footprint for example is commonly less than 100 km wide, (2) how the phenomena relate to isobaric patterns and curvature – CJ strength for example is greatest when the responsible low is moving rapidly as that reduces trajectory curvature, and (3) the different boundary layer structures that are associated. For (3), a fundamental point addressed is how boundary layer configuration, in particular stability, influences gust magnitude at the surface, and we expanded this discussion to look qualitatively at coastal versus inland sites, and day versus night. These distinctions do not have much relevance for SJ cases, but for WJ and CJ cases gusts are generally highest on windward coasts, and for CJ cases inland sites often see higher gusts during the early afternoon. Most of the time in the WJ and CJ environments a restorative buoyancy force precludes the downward propagation of momentum through the lower troposphere, providing protection from damage at the surface. Observations show that only when this process is challenged via convection, of various forms (as in the early afternoon CJ scenario), does one see significant surface gusts from these phenomena.

In the WJ, SJ and CJ categories, we found 11, 13 and 26 probable cases, respectively (Table 1), but it should be stressed that these numbers do not reflect relative frequency, but more the propensity for the phenomena in question to give rise to noteworthy damage. The WJ is without doubt much more common than the SJ.

So whilst the SJ is very rare, it is overall the most damaging phenomenon, and for this reason has been discussed extensively in this paper. From the point of view of surface impact a fundamental point seems to be that the downward propagation of momentum within the SJ proceeds unhindered, as surface observations seem to show, unlike the standard WJ and CJ cases. In part, this descent is dynamically driven. However, it seems that one or two physical processes also play a key role, permitting downwards slantwise convection to occur in a pulsed form. These processes simply cause the descending parcels to acquire a lower potential temperature than their environment. The first process relies on SJ pulses propagating forwards relative to the cyclone (as imagery shows), through a region of broadscale cold advection, to arrive in a warmer environment. The second process relies on evaporation within the parcels themselves (particularly from the ice phase) lowering the potential temperature of those parcels. Evidently both processes would increase DCAPE/DSCAPE, and so *assist* the downward motion, but it does not seem to

be *necessary* to have both for a destructive SJ to be realised. One should suffice. Though there have been signs of evaporation at work in our cases it has not been possible to ascertain how important this process actually is in the lower troposphere. In fact, its importance probably varies between cases. This might also help explain the seemingly inconsistent signals regarding evaporation seen in the literature.

For many new cases, we have now seen supporting evidence in imagery for the SJ phenomenon, namely evaporating filaments of cloud particulate, and gaps in between, that both emanate from the tip of the cloud head, as noted first by Browning (2004) in his analysis of the October87 windstorm. Another key point regarding SJs is their sudden onset; this is one of many aspects that make arriving at correct forecasts extremely difficult.

For SJ cases, the lateral extent of the cloud head filaments and gaps, and the number of them, vary between cases. Larger systems such as October87 and Anatol had many filaments that extended across some distance, whilst smaller lows like Xola and Renate had only one short filament/gap combination. In practice, the strongest gusts are seen downstream of the gaps; this new result is supported by analysis of many cyclones (Oratia, Renate, Xola, Ulli, Christian) and by simulation of Ulli with a 4-km resolution model. Surface footprints denoting SJ damage were typically less than 100 km wide, though this varies between cases, according to cyclone size and the number of filaments/gaps in the cloud head tip.

Whilst progress has been made here in documenting the SJ phenomenon in many new cases, and here and elsewhere in describing the processes that are probably at work, it is important to also recognise that challenges remain. Such is the rarity of SJs that to the authors' knowledge there has yet to be a case that has been well observed in three dimensions whilst extreme gusts were being registered at the surface. One should retain an open mind regarding what such measurements may in future reveal. Within a sting jet zone, the flow may be very unbalanced, and from a modelling perspective normal boundary layer concepts could well break down. The best observational evidence to date was arguably provided by Doppler radar scans of Xola (in Pinto and Silva, 2010), which showed a jet core deep down into the nominal boundary layer, centred at or below 550 m.

Note also that in many past studies the presence of a sting jet has been based on analysis of backward trajectories that began above the nominal boundary layer, from 850 hPa for example. In the present study, the approach has been much more pragmatic and based much more on surface observations, and there will not be perfect agreement between the different approaches regarding classification. If surface impact is important, however, which is true for almost all users, then it is clearly important to refer to surface observations and to understand the related boundary layer behaviour. In this regard, we would also urge caution when using plan-view plots of wind speeds at lower tropospheric levels such as 850 hPa to imply/infer surface gusts; for WJs surface gusts will usually be much less than the value shown, for SJs however they could be greater. Our recommendation also concurs with operational forecasting practice. At the Met Office for example it would be rare for a forecaster to examine levels as high as 850 hPa when attempting to predict surface gusts. Indeed to complement derived model gust output (e.g. as represented on Fig. 10c and d) forecasters commonly refer to model level winds 600 m above the surface as a guide to gusts, with the option to multiply those by a lower tropospheric stability factor ( $\leq 1$). This cautionary note regarding using the 850-hPa wind speed as a storm metric applies equally to IMILAST: standard track datasets for the project include up to three user-specified metrics, and in some instances 850 hPa wind is one of those.

One might also ask if the results of this study apply in other extra-tropical regions. As physics are universal, one would expect some consistency. However, we acknowledge that consensus in this matter is lacking – for example Mass and Dotson (2010) examined a number of cases in the Pacific northwest of America using satellite imagery, Doppler radar, surface observations and high-resolution model simulations, yet could find no evidence of SJ phenomena, and indeed proposed a model of cyclone-related wind maxima that differs somewhat from ours. Notably in their model peak winds coincide with maxima in geostrophic wind speed and curvature, rather than occurring ahead of them.

Another interesting question is 'could a relatively modest cyclone ever have a relatively modest SJ associated, and would imagery signatures ever pinpoint one of these?' The authors are unaware of any such case; more modest cyclones tend not to have a cloud head associated, or if they do the cloud head tip region is ill-defined and inert, with no sign of 'smoking gun' activity. For modest cyclones, the physical processes and dynamics are probably not active enough to permit significant vertical motion couplets near to the surface, as required for the SJ.

With regard to model representation, we have focussed on how well the state-of-the-art and very widely used ERA-I re-analysis (80 km resolution) replicates cyclonic windstorms, partly because this has also been a key component in IMILAST (Table 4). For most large systems (Kyrill being one example), its performance is probably satisfactory, but for the more extreme cyclones, particularly smaller ones, depth and gradients and wind gusts are all underestimated, sometimes to the point where the cyclone is not even noteworthy. Such weaknesses seem to be especially

prominent during the SJ or early CJ phases of the cyclone life-cycle, with the maximum 6-hourly deepening rate, that commonly coincides, typically being underestimated by 25 to 50%. Reasons for these issues are many, though a fundamental one is resolvability: the breadth of the SJ footprint for example (see Table 2) is often close to or less than the ERA-I grid spacing. Note also that current generation global climate models have a resolution that is even lower (around 150 km at best), and consequently their ability to generate realistic windstorms will be compromised even more. At the time of maximum depth for each ISD cyclone we found that depth errors in ERA-I ranged from $-1$ to $+17$ hPa, with a mean of $+4$ hPa.

So an important question is what model resolution does one need to satisfactorily represent an extra-tropical cyclonic windstorm? This depends of course on system size but based on analysis of one fairly typical system (Ulli), that started out small but grew to have largest closed isobar dimensions of about 1000 km some 15 hours after the SJ phase, it seems that horizontal resolution of 20 km or better would be satisfactory. With this, one can capture the gradient magnitude and low depth, and given a satisfactory gust parameterisation, the gust magnitude can be reasonable too. However, if one wishes to capture very small cyclones such as Lothar, Renate and Xola, that can be equally intense, a resolution of 10 km or better may well be required. The breadth of the SJ footprint for Xola, that had extreme 100–125 kt gusts associated, was only about 25 km. Similarly if there is interest in capturing fine-scale details for *any* system, such as the filaments/gaps that make up the cloud head tip, and associated SJ gust maxima at the surface, then resolution of better than 10 km is probably essential. Model simulations at 12 km resolution in Clark et al. (2005) and Martinez-Alvarado et al. (2014) for October87 and Friedhelm, respectively, both provided hints of such structures. Meanwhile in output of an operational Met Office limited area model simulation of Ulli we saw encouraging signs that the relevant processes and patterns can be captured well at 4 km resolution.

With regard to vertical resolution, Clark et al. (2005) suggest that 90 levels or more are needed to resolve the SJ. Reassuringly many operational global models have now reached or exceeded that level, although the ERA-I model version had 60 such levels, which will also not have helped with its representation of the ISD cases with SJs. As regards model time steps, the very rapid onset of the SJ phenomenon is a concern. An amplification of the maximum lower tropospheric wind speed of about 30 kts/h was seen for one case. Such rapid changes bring the potential for model instabilities to break out, and this probably needs further investigation. Similarly if one wants to resolve filamentation processes and pulsing in the SJ domain very short time steps would be essential.

We have to accept that cyclone representation in the ERA-I dataset, and indeed in global climate models, has some significant limitations, which clearly impacts on IMILAST and other studies. For example, using model-based metrics to extricate the most damaging cases from a large sample is unlikely to be particularly successful. Similarly, when comparing tracks derived manually with tracks derived automatically, as has been done in IMILAST, one should keep in mind that discrepancies (in for example wind metrics, central pressures, deepening rates) might owe their existence as much to the re-analysis deficiencies as to artefacts of the specific tracking method. Nevertheless it is not unreasonable to suppose that the behaviour of cyclone tracking algorithms in this framework will not be compromised too much, except of course for very small cyclones that may themselves be unresolved. Indeed this is borne out somewhat by early results from IMILAST which hinted at rather less variability in algorithm behaviour for more substantial cyclones than for cyclones in general.

It is important also to reiterate here that our conceptual model (in Fig. 1 and Table 2), which is a key output of this paper, provides just a general framework, and that details can differ greatly from one damaging cyclone to another. Such differences include, but are not limited to, cyclone and footprint sizes, track length, tracks that do not curve poleward, cyclones that do not decelerate substantially in the CJ phase, flow modulation by topographic features, meso-lows within the main cyclone circulation (e.g. Xaver, see Hewson et al., 2014), localised upright convection in the SJ region (e.g. October87, see Browning, 2004), complex central pressure evolutions (e.g. Kyrill, see Fink et al., 2009), and double frontal structures (e.g. Erwin, see Baker, 2009). On the latter point, a recent study by Mulqueen and Schultz (2015) suggests that multiple frontal structures are commonplace for deep cyclones, at least on manually produced Met Office synoptic charts. However, whilst many of our ISD cases had multiple structures early in their life cycles, few retained these as rapid deepening ensued. Erwin was the main exception.

Many of the complications listed above could provide fruitful areas for future study. It might be especially illuminating to determine what aspects of the atmospheric configuration and related dynamics pre-dispose a cyclone to not slow down markedly after deepening, and to not turn polewards. Both such behaviours enhance the likelihood of very strong winds affecting populated regions. Similarly, further work is needed to better represent complex boundary layer behaviour, and to then get better surface gust estimates from models, especially for inland sites where impacts are greatest. Fig. 10, based on output from two modelling centres (ECMWF and Met Office), suggested that gust representation in a SJ region tends to be good if the driving model has the correct cyclone depth evolution,

though gust details in amongst the complex topography of southern Scotland were not investigated. It is still not entirely clear whether the tendency for substantial SJ gusts to progress across inland sites in a relatively unimpeded way (unlike CJ and WJ gusts) is something that models can capture well. And even at kilometre-scale resolution gust representation seems to be equally problematic, if not more so (Jorge Bornemann, Met Office, personal communication). Finally we would remark that there is one relatively untapped resource for windstorm study over the ocean, which is satellite-based scatterometer data. Such instruments sense capillary waves on the ocean and accordingly provide instantaneous ( $\sim$2 seconds) wind speed estimates (for examples see Mass and Dotson, 2010; Schultz and Sienkiewicz, 2013). Although there are upper limits on speed retrieval, and coverage is discontinuous, deriving windstorm climatologies from the satellite swaths, to compare with models and re-analyses, does have the potential to provide further useful insights.

Our characterisation of windstorms can also help in many ways with future IMILAST-related activities. We have shown for example that extreme cyclones over Europe tend to not be particularly large, tend to not be particularly long-lived, can sometimes move very rapidly, and tend to generate extreme winds only for a matter of hours. Settings in tracking algorithms, such as thresholds, may need to be further adapted to successfully cater for all these factors. Without this recognition, there is a danger of key cyclones being discarded during processing, and then of incorrect conclusions being arrived at regarding, for example, climate change. With regard to extreme wind duration, one should also aim to use as high a temporal resolution in the input data as possible. ERA-I for example provides analysis fields at 6-hour intervals, though intermediate 3-hourly forecast fields are usefully also available. These various concerns will come to the fore even more in future as the models' intrinsic temporal and spatial resolutions increase. Algorithms must be carefully adjusted to ensure that they fully embrace the much improved representivity that should result.

We have described in this paper the overall structure of and motivation for IMILAST, and have highlighted the main results to date, as well as some future directions for project work. On the horizon also are new re-analyses, such as ERA5, which will be the 'satellite-era' successor to ERA-I and which is expected to become available late in 2016. This will run at a horizontal resolution of 40 km or better, and will have the added benefit of ensemble data assimilation, which should allow for better use of and acceptance of observational data in dynamically active environments, such as those that lead up to and include cyclonic windstorms. It will be interesting to revisit the ISD to see how much ERA5 improves representation. Providing care is taken to adapt algorithms to this higher resolution this should be relatively straightforward. Although 40 km falls short of our proposed target resolution of 10–20 km we nonetheless anticipate a substantial improvement in quality.

## 7. Acknowledgements

The Met Office is gratefully acknowledged as the source of gust plots in Fig. 4a (updated using data in McCallum, 1990) and 4b, data in Fig. 9a and b, and Met Office model output used in Fig. 10. Thanks to Peter Sloss from Aberdeen Weather Centre for feedback regarding cyclone Ulli, and for related gust return periods. Philippe Arbogast of Météo-France provided data input to Fig. 4c, whilst EUMETSAT was the source of imagery shown in Fig. 9. The Meteorology department at Reading University took measurements used in Fig. 3. We thank Rob Wilbraham of the Met Office for his diligence in putting together the cyclone best-track dataset, and Deutscher Wetterdienst for also providing manual tracks for the ISD. The manuscript also benefitted from discussions at ECMWF with Fernando Prates (windstorm Xola) and Paul Poli (assimilation issues). Swiss Re is acknowledged for its support of the project IMILAST.

## References

Agustí-Panareda, A., Gray, S. L., Craig, G. C. and Thorncroft, C. 2005. The extratropical transition of Tropical Cyclone Lili (1996) and its crucial contribution to a moderate extratropical development. *Mon. Weather Rev.* **133**, 1562–1573.

Akperov, M. G., Bardin, M. Yu., Volodin, E. M., Golitsyn, G. S. and Mokhov, I. I. 2007. Probability distributions for cyclones and anticyclones from the NCEP/NCAR reanalysis data and the INM RAS climate model. *Izvest. Atmos. Ocean. Phys.* **43**, 705–712.

Baehr, C., Pouponneau, B., Ayrault, F. and Joly, A. 1999. Dynamical Characterization of the FASTEX cyclogenesis cases. *Q. J. Roy. Meteorol. Soc.* **125**, 3469–3494.

Baker, L. 2009. Sting jets in severe northern European wind storms. *Weather*. **64**, 143–148.

Baker, L., Martinez-Alvarado, O., Methven, J. and Knippertz, P. 2013. Flying through extratropical cyclone Friedhelm. *Weather*. **68**, 9–13.

Benestad, R. E. and Chen, D. 2006. The use of a calculus-based cyclone identification method for generating storm statistics. *Tellus A*. **58**, 473–486.

Bertotti, L., Bidlot, J.-R., Bunney, C., Cavaleri, L., Delli Passeri, L. and co-authors. 2012. Performance of different forecast systems in an exceptional storm in the Western Mediterranean Sea. *Q. J. Roy. Meteorol. Soc.* **138**, 34–55.

Blender, R., Fraedrich, K. and Lunkeit, F. 1997. Identification of cyclone-track regimes in the North Atlantic. *Q. J. Roy. Meteorol. Soc.* **123**, 727–741.

Browning, K. A. 2004. The sting at the end of the tail: damaging winds associated with extratropical cyclones. *Q. J. Roy. Meteorol. Soc.* **130**, 375–399.

Browning, K. A. 2005. Observational synthesis of mesoscale structures within an explosively developing cyclone. *Q. J. Roy. Meteorol. Soc.* **131**, 603–623.

Burt, S. D. and Mansfield, D. A. 1988. The great storm of 15–16 October 1987. *Weather*. **43**, 90–110.

Caspar, R., Costa, S. and Jakob, E. 2007. Fronts froids et submersions de tempête dans le nord-ouest de la France: Le cas des inondations par la mer entre l'estuaire de la Seine et la baie de Somme [A case of coastal flooding between the estuary of the Seine river and the bay of the Somme]. *La Meteorol.* **57**, 37–47.

Clark, P. A., Browning, K. A. and Wang, C. 2005. The sting at the end of the tail: model diagnostics of fine-scale three-dimensional structure of the cloud head. *Q. J. Roy. Meteorol. Soc.* **131**, 2263–2292.

Dee, D. P., Uppala, S. M., Simmons, A. J., Berrisford, P., Poli, P. and co-authors. 2011. The ERA-interim reanalysis: configuration and performance of the data assimilation system. *Q. J. Roy. Meteorol. Soc.* **137**, 553–597.

Deroche, M.-S., Choux, M., Codron, F. and Yiou, P. 2014. Three variables are better than one: detection of European winter windstorms causing important damages. *Nat. Hazards Earth Syst. Sci.* **14**, 981–993.

Fink, A. H., Brücher, T., Ermert, V., Krüger, A. and Pinto, J. G. 2009. The European storm Kyrill in January 2007: synoptic evolution, meteorological impacts and some considerations with respect to climate change. *Nat. Hazards Earth Syst. Sci.* **9**, 405–423.

Fox, A., Sherwin, R. and Ralston, F. 2012. Lessons learnt at the Met Office from the great storm of 1987 – a comparison with recent strong wind events. *Weather*. **67**, 268–273.

Franklin, J. L. and Brown, D. P. 2008. Atlantic hurricane season of 2006. *Mon. Weather Rev.* **136**, 1174–1200.

Gray, S. L., Martinez-Alvarado, O., Baker, L. H. and Clark, P. A. 2011. Conditional symmetric instability in sting-jet storms. *Q. J. Roy. Meteorol. Soc.* **137**, 1482–1500.

Hanley, J. and Caballero, R. 2012. Objective identification and tracking of multicentre cyclones in the ERA-Interim reanalysis data set. *Q. J. Roy. Meteorol. Soc.* **138**, 612–625.

Heming, J. T. 1990. The impact of surface and radiosonde observations from two Atlantic ships on a numerical weather prediction model forecast for the storm of 25 January 1990. *Meteorol. Mag.* **119**, 249–259.

Hewson, T. D. 1998. Objective fronts. *Meteorol. Appl.* **5**, 37–65.

Hewson, T. D. 2001. The North Sea storm of 30 October 2000. *Weather*. **56**, 115–116.

Hewson, T. D. 2009. Diminutive frontal waves – a link between fronts and cyclones. *J. Atmos. Sci.* **66**, 116–132.

Hewson, T. D. and Titley, H. A. 2010. Objective identification, typing and tracking of the complete life-cycles of cyclonic features at high spatial resolution. *Meteorol. Appl.* **17**, 355–381.

Hewson, T. D., Magnusson, L., Breivik, O., Prates, F., Tsonevsky, I., and de Vries, J. W. 2014. Windstorms in northwest Europe in late 2013. *ECMWF Newslett.* **139**, 122–128.

Hodges, K. I. 1995. Feature tracking on the unit sphere. *Mon. Weather Rev.* **123**, 3458–3465.

Inatsu, M. 2009. The neighbor enclosed area tracking algorithm for extratropical wintertime cyclones. *Atmos. Sci. Lett.* **10**, 267–272.

Joyner, T. A. 2013. Optimizing peak gust and maximum sustained wind speed estimates from mid-latitude wave cyclones. PhD Dissertation. Louisiana State University. Online at: etd.lsu.edu/docs/available/etd-04052013-150210/

Kew, S. F., Sprenger, M. and Davies, H. C. 2010. Potential vorticity anomalies of the lowermost stratosphere: a 10-yr winter climatology. *Mon. Weather Rev.* **138**, 1234–1249.

Lamb, H. H. 1991. *Historic Storms of the North Sea, British Isles and Northwest Europe*. Cambridge University Press, Cambridge, UK.

Liberato, M. R. L., Pinto, J. G., Trigo, I. F. and Trigo, R. M. 2011. Klaus – an exceptional winter storm over northern Iberia and southern France. *Weather*. **66**, 330–334.

Lionello, P., Dalan, F. and Elvini, E. 2002. Cyclones in the Mediterranean region: the present and the doubled CO2 climate scenarios. *Clim. Res.* **22**, 147–159.

Lumbroso, D. M. and Vinet, F. 2011. A comparison of the causes, effects and aftermaths of the coastal flooding of England in 1953 and France in 2010. *Nat. Hazards Earth Syst. Sci.* **11**, 2321–2333.

Martínez-Alvarado, O., Baker, L. H., Gray, S. L., Methven, J. and Plant, R. S. 2014. Distinguishing the cold conveyor belt and sting jet airstreams in an intense extratropical cyclone. *Mon. Weather Rev.* **142**, 2571–2595.

Martinez-Alvarado, O., Gray, S. L., Catto, J. L. and Clark, P. A. 2012. Sting jets in intense winter North-Atlantic windstorms. *Environ. Res. Lett.* **7**: 024014, DOI: 10.1088/1748-9326/7/2/024014.

Martínez-Alvarado, O., Weidle, F. and Gray, S. L. 2010. Sting jets in simulations of a real cyclone by two mesoscale models. *Mon. Weather Rev.* **138**, 4054–4075.

Mass, C. F. 1991. Synoptic frontal analysis: time for a reassessment? *Bull. Am. Meteorol. Soc.* **72**, 348–363.

Mass, C. F. and Dotson, B. 2010. Major extratropical cyclones of the Northwest United States: historical review, climatology, and synoptic environment. *Mon. Weather Rev.* **138**, 2499–2527.

McCallum, E. 1990. The burns' day storm, 25 January 1990. *Weather*. **45**, 166–173.

McCallum, E. and Norris, W. J. T. 1990. The storms of January and February 1990. *Meteorol. Mag.* **119**, 201–210.

Mitchell-Wallace, K. and Mitchell, A. 2007. *Windstorm Kyrill, 18 January 2007*. Report of the Willis Research Network. 21 p. Online at: www.willisresearchnetwork.com/assets/templates/wrn/files/Willis Windstorm Kyrill Report 01 Feb 2007.pdf

Mulqueen, K. and Schultz, D. 2015. Nonclassical extratropical cyclones on Met Office sea-level pressure charts: double cold and warm fronts. *Weather*. **70**, 100–105.

Murray, R. J. and Simmonds, I. 1991. A numerical scheme for tracking cyclone centres from digital data. Part I: development and operation of the scheme. *Aust. Meteorol. Mag.* **39**, 155–166.

Neu, U., Akperov, M. G., Bellenbaum, N., Benestad, R., Blender, R. and co-authors. 2013. IMILAST: a community effort to intercompare extratropical cyclone detection and tracking algorithms. *Bull. Am. Meteorol. Soc.* **94**, 529–547.

Nielsen, N. W. and Sass, B. H. 2003. A numerical, high-resolution study of the life cycle of the severe storm over Denmark on 3 December 1999. *Tellus A*. **55**, 338–351.

Panofsky, H. A., Tennekes, H., Lenschow, D. H. and Wyngaard, J. C. 1977. The characteristics of turbulent velocity components in the surface layer under convective conditions. *Bound. Layer Meteorol.* **11**, 355–361.

Parton, G., Dore, A. and Vaughan, G. 2010. A climatology of mid-tropospheric mesoscale strong wind events as observed by the MST radar, Aberystwyth. *Meteorol. Appl.* **17**, 340–354.

Parton, G. A., Vaughan, G., Norton, E. G., Browning, K. A. and Clark, P. A. 2009. Wind profiler observations of a sting jet. *Q. J. Roy. Meteorol. Soc.* **135**, 663–680.

Pearce, R., Lloyd, D. and McConnell, D. 2001. The post-Christmas 'French' storms of 1999. *Weather*. **56**, 81–91.

Pedgley, D. E. 1997. The fastnet storm of 1979: a mesoscale surface jet. *Weather*. **52**, 230–242.

Pinto, P. and Silva, A. 2010. *Situação de vento forte no Oeste em 23 de Dezembro de 2009* [The strong wind event of 23rd December 2009 in the Oeste region of Portugal]. Report from Instituto Português do Mar e da Atmosfera. 40 p (in Portuguese). Online at: www.ipma.pt/resources.www/docs_pontuais/ocorrencias2009/RelVentoOeste.pdf

Prahl, B. F., Rybski, D., Burghoff, O. and Kropp, J. P. 2015. Comparison of storm damage functions and their performance. *Nat. Hazards Earth Syst. Sci.* **15**, 769–788.

Raible, C. C., Della-Marta, P. M., Schwierz, C., Wernli, H. and Blender, R. 2008. Northern Hemisphere extratropical cyclones: a comparison of detection and tracking methods and different reanalyses. *Mon. Weather Rev.* **136**, 880–897.

Roberts, J. F., Champion, A. J., Dawkins, L. C., Hodges, K. I., Shaffrey, L. C. and co-authors. 2014. The XWS open access catalogue of extreme European windstorms from 1979 to 2012. *Nat. Hazards Earth Syst. Sci.* **14**, 2487–2501.

Rudeva, I. and Gulev, S. K. 2007. Climatology of cyclone size characteristics and their changes during the cyclone life cycle. *Mon. Weather Rev.* **135**, 2568–2587.

Sanders, F. and Gyakum, J. R. 1980. Synoptic-dynamic climatology of the "bomb". *Mon. Weather Rev.* **108**, 1589–1606.

Schultz, D. M. and Sienkiewicz, J. M. 2013. Using frontogenesis to identify sting jets in extratropical cyclones. *Weather Forecast.* **28**, 603–613.

Schultz, D. M. and Vaughan, G. 2011. Occluded fronts and the occlusion process: a fresh look at conventional wisdom. *Bull. Am. Meteorol. Soc.* **92**, 443–466.

Schultz, D. M. and Zhang, F. 2007. Baroclinic development within zonally-varying flows. *Q. J. Roy. Meteorol. Soc.* **133**, 1101–1112.

Serreze, M. C. 1995. Climatological aspects of cyclone development and decay in the Arctic. *Atmos. Ocean.* **33**, 1–23.

Shapiro, M. A. and Keyser, D. 1990. Fronts, jet streams and the tropopause. In: *Extratropical Cyclones, The Erik Palmén Memorial Volume* (eds. C. W. Newton and E. O. Holopainen). American Meteorological Society, Boston, MA, pp. 167–191.

Shutts, G. J. 1990. Dynamical aspects of the October storm, 1987: a study of a successful fine-mesh simulation. *Q. J. Roy. Meteorol. Soc.* **116**, 1315–1347.

Simmonds, I., Murray, R. J. and Leighton, R. M. 1999. A refinement of cyclone tracking methods with data from FROST. *Aust. Meteor. Mag.* **Special Issue:** 35–49.

Sinclair, M. R. 1997. Objective identification of cyclones and their circulation intensity, and climatology. *Weather Forecast.* **12**, 591–608.

Smart, D. J. and Browning, K. A. 2014. Attribution of strong winds to a cold conveyor belt and sting jet. *Q. J. Roy. Meteorol. Soc.* **140**, 595–610.

Trigo, I. F. 2006. Climatology and interannual variability of storm-tracks in the Euro-Atlantic sector: a comparison between ERA-40 and NCEP/NCAR reanalyses. *Clim. Dyn.* **26**, 127–143.

Tripoli, G. J., Medaglia, C. M., Dietrich, S., Mugnai, A., Panegrossi, G. and co-authors. 2005. The 9–10 November 2001 Algerian flood: a numerical study. *Bull. Am. Meteorol. Soc.* **86**, 1229–1235.

Ulbrich, U., Fink, A. H., Klawa, M. and Pinto, J. G. 2001. Three extreme storms over Europe in December 1999. *Weather*. **56**, 70–80.

Ulbrich, U., Leckebusch, G. C., Grieger, J., Schuster, M., Akperov, M. and co-authors. 2013. Are greenhouse gas signals of Northern Hemisphere winter extra-tropical cyclone activity dependent on the identification and tracking algorithm? *Meteorol. Z.* **22**, 61–68.

Ulbrich, U., Leckebusch, G. C. and Pinto, J. G. 2009. Extra-tropical cyclones in the present and future climate: a review. *Theor. Appl. Climatol.* **96**, 117–131.

Vaughan, G., Methven, J., Anderson, D., Antonescu, B., Baker, L. and co-authors. 2014. Cloud banding and winds in intense European cyclones: results from the DIAMET project. *Bull. Am. Meteorol. Soc.* **96**, 249–265.

Wales Online. 2010. Heavy rain and gale-force winds leave trail of destruction. Online at: www.walesonline.co.uk/news/wales-news/heavy-rain-gale-force-winds-leave-1908460

Wernli, H., Dirren, S., Liniger, M. A. and Zillig, M. 2002. Dynamical aspects of the life cycle of the winter storm 'Lothar' (24–26 December 1999). *Q. J. Roy. Meteorol. Soc.* **128**, 405–429.

Wernli, H. and Schwierz, C. 2006. Surface cyclones in the ERA-40 dataset (1958–2001). Part I: novel identification method and global climatology. *J. Atmos. Sci.* **63**, 2486–2507.

Young, M. V. 1990. Satellite and radar images, 0900 GMT on 3 February 1990. *Weather*. **45**, 268–270.

Young, M. V. and Grahame, N. S. 1999. Forecasting the Christmas eve storm 1997. *Weather*. **54**, 382–391.